Chapter 19
Icy Satellites of Saturn: Impact Cratering and Age Determination

Luke Dones, Clark R. Chapman, William B. McKinnon, H. Jay Melosh, Michelle R. Kirchoff,
Gerhard Neukum, and Kevin J. Zahnle

Abstract Saturn is the first giant planet to be visited by an orbiting spacecraft that can transmit large amounts of data to Earth. Crater counts on satellites from Phoebe inward to the regular satellites and ring moons are providing unprecedented insights into the origin and time histories of the impacting populations. Many Voyager-era scientists concluded that the satellites had been struck by at least two populations of impactors. In this view, the Population I impactors, which were generally judged to be "comets" orbiting the Sun, formed most of the larger and older craters, while Population II impactors, interpreted as Saturn-orbiting ejecta from impacts on satellites, produced most of the smaller and younger craters. Voyager data also implied that all of the "ring moons," and probably some of the mid-sized classical moons, had been catastrophically disrupted and reaccreted since they formed. We examine models of the primary impactor populations in the Saturn system. At the present time, "ecliptic comets," which likely originate in the Kuiper Belt/Scattered Disk, are predicted to dominate impacts on the regular satellites and ring moons, but the models require extrapolations in size (from the observed Kuiper Belt Objects to the much smaller bodies that produce the craters) or in distance (from the known active Jupiter family comets to 9.5 AU). Phoebe, Iapetus, and perhaps even moons closer to Saturn have been struck by irregular satellites as well. We describe the Nice model, which provides a plausible mechanism by which the entire Solar System might have experienced an era of heavy bombardment long after the planets formed. We then discuss the three cratering chronologies, including one based upon the Nice model, that have been used to infer surface ages from crater densities on the saturnian satellites. After reviewing scaling relations between the properties of impactors and the craters they produce, we provide model estimates of the present-day rate at which comets impact, and catastrophically disrupt, the saturnian moons. Finally, we present crater counts on the satellites from two different groups. Many of the heavily cratered terrains appear to be nearly saturated, so it is difficult to infer the provenance of the impactors from crater counts alone. More large craters have been found on Iapetus than on any other satellite. Enceladus displays an enormous range of surface ages, ranging from the old mid-latitude plains to the extremely young South Polar Terrain. Cassini images provide some evidence for the reality of "Population II". Most of the observed craters may have formed in one or more "cataclysms," but more work is needed to determine the roles of heliocentric and planetocentric bodies in creating the craters.

L. Dones and C.R. Chapman
Southwest Research Institute, Boulder, CO 80302, USA

W.B. McKinnon
Washington University in Saint Louis, St. Louis, MO 63130, USA

H.J. Melosh
University of Arizona, Tucson, AZ 85721, USA
Now at Purdue University, West Lafayette, IN 47907

M.R. Kirchoff
Lunar and Planetary Institute, Houston, TX 77058, USA
Now at Southwest Research Institute, Boulder CO 80302, USA

G. Neukum
Freie Universität, 12249 Berlin, Germany

K.J. Zahnle
NASA Ames Research Center, Moffett Field, CA 94035, USA

19.1 Introduction: Understanding of Saturnian Impact Crater Populations Through the Voyager Era

During the three centuries following the discovery of Titan by Christiaan Huygens and Iapetus, Rhea, Tethys, and Dione by Gio Domenico Cassini, the nature of these moons' surfaces was unknown. Ostro and Pettengill (1978) had concluded that the "anomalous" radar behavior of Europa, Ganymede, and Callisto could be explained if these moons had icy, cratered surfaces, Nonetheless, the existence of macroscopic craters on icy satellites remained uncertain because of doubts about whether ice could support topography over geological timescales. Torrence Johnson wrote (Johnson 1978):

> We do not know what the satellite surfaces look like, whether there are craters, mountains, rifts, or new and unexpected tectonic features.

M.K. Dougherty et al. (eds.), *Saturn from Cassini-Huygens*,
DOI 10.1007/978-1-4020-9217-6_19,

The Voyagers, of course, discovered craters on every satellite they imaged at sufficient resolution (with the singular exception of Io). Early Voyager studies of the saturnian satellites in particular (Smith et al. 1981, 1982) proposed that there were two sources of bodies responsible for the visible craters in that system. The earlier impactors, "Population I," most clearly expressed on Rhea, were "characterized by a relatively high abundance of craters larger than ∼20 km" (Smith et al. 1981), with a size-frequency distribution (SFD) crudely similar to the SFDs on the Moon and terrestrial planets. However, Population I was thought to have been formed by "debris in heliocentric orbits," i.e., "comets".[1] "Population II" appeared on the younger (i.e., less cratered) terrains on Dione and Tethys, dominated Mimas and (apparently) Enceladus (where craters could be seen at all), and featured "abundant craters smaller than ∼20 km and a general absence of larger craters" (Smith et al. 1981). Population II craters were generally taken to have been formed by circum-Saturnian debris from the cratering or breakup of adjacent satellites, although Plescia and Boyce (1985) took them to be late-arriving bodies from heliocentric orbit. These attributes of Saturn satellite SFDs were further documented by crater statistics published by Strom (1981) and others and were summarized by Chapman and McKinnon (1986). The reality of the two populations was questioned by Lissauer et al. (1988), who argued instead that all of the craters could be explained by saturation equilibrium by a single population of heliocentric comets rich in small bodies, although their crater statistics show significant differences between Rhea and Mimas. Cratering of Mimas was later modeled by Chapman (1990) using Population II characteristics very different from Population I.

Voyager-era estimates of cratering rates at Saturn were given by Smith et al. (1981, 1982) and by Shoemaker and Wolfe (1981). These authors estimated that "Saturn-family" comets (a population akin to what we now call ecliptic comets; see Section 19.2) dominated cratering on Rhea and moons interior to its orbit, while Oort Cloud comets dominated on moons further from Saturn. This calculation was based on the only Saturn-family "comet" known at that time, the 140-km-diameter Chiron, which had been discovered in 1977 (and is now known as the first Centaur to be found). According to these rate estimates, cratering at the present-day rate could have not produced the observed number of craters on most of the terrains observed by Voyager in the age of the Solar System. Presumably, then, there was an intense early bombardment of the satellites, which might or might not be related to the lunar Late Heavy Bombardment (LHB), i.e., the formation of large basins such as Imbrium and Orientale some 3.8–3.9 billion years ago (Hartmann et al. 2000; Chapman et al. 2007).

Besides these a priori estimates, cratering rates can be scaled from moon to moon, allowing for the higher spatial densities and velocities of (heliocentric) impactors closer to Saturn due to gravitational focusing. Scaling from Iapetus' cratering record, Smith et al. (1982) inferred that all the moons interior to Dione's orbit should have been catastrophically disrupted one or more times. Here catastrophic disruption was equated with the formation of a crater whose diameter equaled the diameter of the satellite. However, the use of Iapetus as a template can be questioned, because Voyager had found, surprisingly, that the density of large craters on Iapetus was slightly higher than on Rhea and Mimas. Models, by contrast, predict much larger cratering rates per unit area on Rhea, Mimas, and the other inner moons than on Iapetus because of gravitational focusing by Saturn (e.g., Zahnle et al. 2003). The Voyager results seem to imply one or more of the following: (1) Iapetus and Rhea were cratered by different populations of impactors; (2) the most heavily cratered terrains on all the moons are saturated; (3) more crater relaxation has taken place on Rhea than on Iapetus; or (4) Rhea's surface is, on average, considerably younger than that of Iapetus (Lissauer et al. 1988).

The key goal of crater counting was expressed by Shoemaker et al. (1963) in the classic paper "Interplanetary Correlation of Geologic Time":

> . . . if the frequency of meteoroid impact and its variation with time on the different planets can be established, the age of rock bodies exposed on their surfaces can be estimated from the distribution of superimposed impact craters.

Hartmann (1965, 1966) used crater counts on the Canadian shield to correctly deduce the age of the lunar maria, and concluded that the average early impact rate on the lunar highlands must have been at least 100 times the present-day rate (Hartmann et al. 2000). Radiometric dating of lunar samples returned by the Apollo astronauts provided an absolute chronology for the Moon, and the lunar chronology was applied to Mars (Neukum and Hiller 1981). Asteroids are the primary impactors on the terrestrial planets, so it is possible to relate their chronologies to each other (Hartmann and Neukum 2001; Strom et al. 2005). However, comets are widely (Smith et al. 1981, 1982; Zahnle et al. 1998, 2003; Schenk et al. 2004), though not universally (Neukum et al. 1998, 1999, 2005, 2006; Schmedemann et al. 2008, 2009) thought to be the main impactors on the giant planets and their satellites. Since no radiometric dates exist for surfaces in the outer Solar System, and the size-frequency distribution of comets is less well understood than that of asteroids, the chronology of the moons of the giant planets remains in a primitive state. Nevertheless, we may rejoice that there are copious impact craters to count, their survival

[1] In this chapter, we use the term "comet" as a generic term for a planetesimal in the region of the giant planets or beyond. By our definition, comets need not have comae.

over geologic time against viscous relaxation now understood (Dombard and McKinnon 2000).

In Section 19.2 we discuss impactor populations; in Section 19.3, recent ideas about the impact flux in the first billion years of Solar System history; in Section 19.4, cratering chronologies; in Section 19.5, impact physics and scaling laws; in Section 19.6, predicted cratering rates; in Section 19.7, observed crater statistics; and in Section 19.8, conclusions.

19.2 Impactor Populations

Potential impactors on the saturnian moons can be divided into six categories.

First, most *main-belt asteroids* follow orbits with average distances from the Sun in the range 2.1–3.3 Astronomical Units (AU) from the Sun. The main belt is estimated to contain of order 10^6 objects with diameters $d > 1$ km (Bottke et al. 2005).

Second, both Jupiter and Neptune have *Trojans*, small bodies that librate around the Lagrangian points some 60° ahead of and behind each planet in its orbit. The number of km-sized Trojans of Jupiter is comparable to the number of main-belt asteroids (Shoemaker et al. 1989; Jewitt et al. 2000). The number of km-sized Neptune Trojans is unknown; it may be far greater than the population of Jupiter Trojans. Because of Neptune's great distance from the Sun, only six of its Trojans, all larger than ∼100 km, have been detected thus far (Sheppard and Trujillo 2006). Although Trojans are sometimes called "Trojan asteroids," these bodies appear to be more closely related to comets than to most main-belt asteroids.[2]

Third, *Centaurs and ecliptic comets*, which are believed to originate in the Kuiper Belt/Scattered Disk[3] (Gladman et al. 2008; Morbidelli et al. 2008; Kenyon et al. 2008; and other chapters in *The Solar System Beyond Neptune* [Barucci et al. 2008]; Jewitt 2008) beyond Neptune's orbit, are generally thought to be the primary impactors on the regular satellites of the giant planets at the present epoch. The Kuiper Belt is estimated to contain nearly 10^5 bodies with diameters, d, larger than 100 km. The Kuiper Belt size distribution flattens markedly at smaller sizes, with a "knee" in the distribution at $d = 90 \pm 30$ km (Fuentes et al. 2009; see Fig. 19.1), where the sizes are derived assuming a representative albedo of 0.04. The smallest body detected in the Kuiper Belt thus far has $d \sim 25$ km (Bernstein et al. 2004). Since impactors from heliocentric orbit typically produce craters larger than the impactors themselves by a factor of 10 or more, our current census of the belt provides little direct information on the size range relevant to cratering the satellites.

Bodies slowly leak from the Kuiper Belt to become "ecliptic comets," which include Scattered Disk Objects with eccentric orbits outside that of Neptune and Centaurs with orbits in the Jupiter-Neptune region (Levison and Duncan 1997; Duncan and Levison 1997; Tiscareno and Malhotra 2003; Duncan et al. 2004; Di Sisto and Brunini 2007; Volk and Malhotra 2008). The steady-state population of Saturn-crossing Centaurs is $\sim 10^{-4}$ times the population of the Kuiper Belt (Irwin et al. 1995; Fig. 19.2)[4]. However, the population of km-sized Kuiper Belt Objects (KBOs) [and hence Centaurs] is highly uncertain; we defer discussion of the absolute number of Saturn-crossing Centaurs to Section 19.6.

More than 300 Jupiter-family comets (JFCs) have been discovered (Fernández 2009). JFCs, which have small orbital inclinations, are thought to be Centaurs that have come close enough to the Sun (typically, perihelion distances <3 AU) that they release gas and dust. Most *known* JFCs have nuclei with diameters in the range 1–10 km; the true size-frequency distribution of JFC nuclei can be approximated by a power law with a possible flattening or cutoff near 1 km (Lamy et al. 2004). Comet Shoemaker-Levy 9 (SL9) was a JFC that was tidally disrupted by Jupiter in 1992; the fragments struck the planet in 1994. Prior to its tidal disruption, the diameter of SL9's nucleus is estimated to have been 1.5–1.8 km (Asphaug and Benz 1996). Zahnle et al. (2003) use the historical rate of close passages of comets such as SL9

[2] We do not break out the Hilda asteroids, a relatively populous group occupying the 3:2 mean-motion resonance with Jupiter (Brunini et al. 2003) separately. For the purposes of this chapter, the Hildas can be considered as a source population combined with either the Trojan asteroids or the ecliptic comets.

[3] For the remainder of this article, we define the Kuiper Belt as the group of small bodies in heliocentric orbit with perihelion distances between 30 and 50 AU, not including Neptune's Trojans. By this definition, the Kuiper Belt includes the "Scattered Disk". The Kuiper Belt appears to be a mix of at least two populations with different dynamical and physical properties, and distinct size-frequency distributions. Duncan et al. (2004) have stated that the Scattered Disk is the primary source of the Centaurs and ecliptic comets (and therefore the cometary impactors on the moons of the giant planets), but the size distributions of the different populations in the Kuiper Belt are not known at most of the sizes relevant for cratering, so this conclusion is premature (Volk and Malhotra 2008).

[4] The number of Jupiter- and Saturn-crossing Centaurs is small because the giant planets quickly eject most bodies that cross their orbits from the Solar System. If N_{Saturn} is the number of Saturn-crossing bodies larger than a given size, N_{KB} is the number of Kuiper Belt Objects larger than that size, and assume no physical disruption of Centaurs, we have $N_{Saturn}/N_{KB} \sim f_{escape}\ f_{Saturn}\ t_{Saturn}/t_{KB}$, where f_{escape} is the fraction that escapes the Kuiper Belt in the age of the Solar System, f_{Saturn} is the fraction of escapees that become planet-crossing, t_{Saturn} is the typical lifetime of Saturn crossers found from numerical orbit integrations, and t_{KB} is the typical lifetime of a Kuiper Belt Object. Taking $f_{escape} = 0.4$, $f_{Saturn} = 0.5$, $t_{Saturn} = 3 \times 10^6$ years, $t_{KB} = 4 \times 10^9$ years, we have $N_{Saturn}/N_{KB} \sim 10^{-4}$ (Irwin et al. 1995).

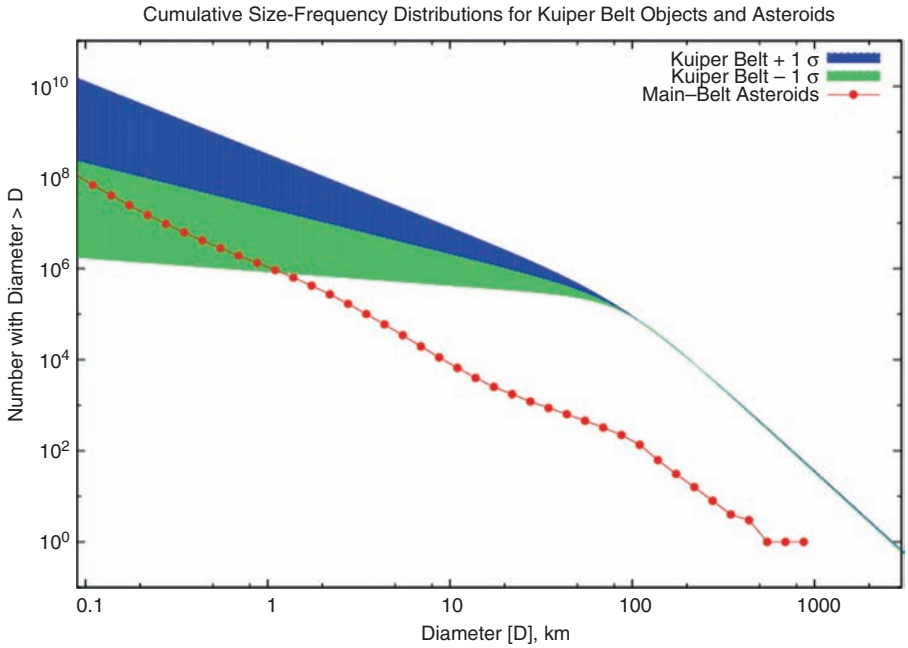

Fig. 19.1 Cumulative size-frequency distribution of Kuiper Belt Objects (*blue and green bands*) from Fuentes et al. (2009) and asteroids (*red dots*) from Bottke et al. (2005). Representative albedos of 0.04 and 0.092 were used to convert the respective absolute magnitude distributions to physical size distributions. The Kuiper Belt size distribution is well constrained only for diameters larger than tens of km, while the asteroidal size distribution is known down to sizes a bit smaller than 1 km (Gladman et al. 2009). The known number of Jupiter-family comets exceeds the range of values predicted by the Fuentes et al. (2009) distribution. The cause of this discrepancy is unknown

to Jupiter, other observations, and the model Centaur orbital distribution from Levison and Duncan (1997) to estimate that 0.003–0.009 ecliptic comets with $d > 1$ km strike Saturn itself per year.

In Fig. 19.1 we show the cumulative size-frequency distributions (SFDs) of Kuiper Belt Objects (Fuentes et al. 2009) and main-belt asteroids (Bottke et al. 2005). The blue and green bands for the Kuiper Belt Objects represent $\pm 1\sigma$ uncertainties. To lowest order, the SFD of Centaurs should be the same as that of KBOs, since Centaurs rarely collide with each other (Durda and Stern 2000). However, some comets split (Boehnhardt 2004) or undergo outbursts (West et al. 1991) at heliocentric distances beyond 10 AU, thereby perhaps changing the SFD of Saturn-crossing bodies. Even ignoring this complication, the uncertainties in Fig. 19.1 are enormous by the time one reaches the km-sized bodies that produce craters with diameters of tens of km in the Saturn system. Kuiper Belt Objects are more numerous than asteroids, at least for bodies larger than about 1 km. The asteroidal size-frequency distribution is well-determined down to 1 km, and uncertain at smaller sizes.

In Fig. 19.2 we show the heliocentric distance distribution, dN/dr, of Centaurs in simulations by Di Sisto and Brunini (2007). The distribution can be approximated by power laws, $dN/dr \propto r^4$ for $r < 30$ AU and $dN/dr \propto r^{-1.5}$ for $r > 30$ AU, in general agreement with Levison and Duncan (1997) and Tiscareno and Malhotra (2003). If

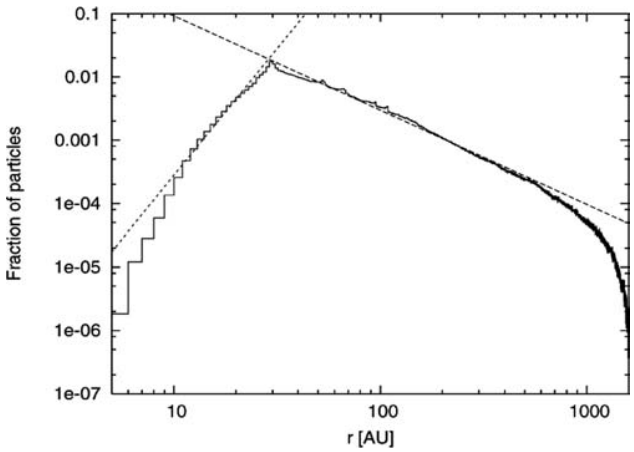

Fig. 19.2 Theoretical radial distribution, dN/dr, of Centaurs and Scattered Disk Objects, from Di Sisto and Brunini (2007). In the region of the giant planets, $r < 30$ AU, the numbers falls steeply inward because gravitational scattering by the giant planets, particularly Jupiter and Saturn, rapidly ejects most planet-crossing small bodies from the Solar System

Centaurs remain intact, the SFD of Centaurs should have the same shape as that in Fig. 19.1, but scaled to each planet by factors given in Fig. 19.2.

Fourth, Saturn's *irregular satellites* follow distant, highly inclined (both prograde and retrograde), eccentric orbits

around the planet. The irregular satellites of the giant planets are thought to have been captured from heliocentric orbit through some form of dissipation such as gas drag, collisions with other small bodies within the Hill sphere of the parent planet (Turrini et al. 2009), or various dynamical "freeze-in" processes (Morbidelli et al. 2005; Vokrouhlický et al. 2008). Until the year 2000, Phoebe, which has an average diameter of 213 km (Thomas et al. 2007b), was the only known saturnian irregular, but a total of 37 are now known (JPL Solar System Dynamics 2009). The newly discovered irregulars have diameters ranging between 4 and 40 km. Many of the irregulars cross each others' orbits, and so can collide. The present-day cratering rate on Phoebe by other irregulars is estimated to be larger than the rate due to ecliptic comets (Nesvorný et al. 2003). Some of Saturn's irregular satellites may belong to collisional families (Turrini et al. 2008) like those in the main asteroid belt (Nesvorný et al. 2002; Parker et al. 2008), Trojan swarms of Jupiter (Shoemaker et al. 1989; Roig et al. 2008), and Kuiper Belt (Brown et al. 2007; Ragozzine and Brown 2007). When the irregulars were captured, their orbits may have extended closer to Saturn (Nesvorný et al. 2007), and these early irregulars might have produced many of the craters on Iapetus, or perhaps even moons closer to Saturn (Bottke et al. 2009; W. F. Bottke and D. Nesvorný, personal communication, 2009). Irregular satellites appear to have a shallow size-frequency distribution, even when observational biases are properly taken into account (Nicholson et al. 2008).

Fifth, *planetocentric bodies* can arise as (a) fragments, launched from cratered or disrupted satellites, which then orbit Saturn for some time, typically decades or hundreds of years, before usually colliding with the satellite from which they were launched (Alvarellos et al. 2005), excepting ejecta from Hyperion (Farinella et al. 1990; Dobrovolskis and Lissauer 2004); (b) comets or asteroids temporarily captured by Saturn, akin to the capture of SL9 by Jupiter (Kary and Dones 1996); (c) bodies captured permanently after tidal disruption (Dones 1991); or (d) asteroids permanently captured by Saturn by some unspecified process (Schmedemann et al. 2008, 2009). Alvarellos et al. (2005) estimate that satellite ejecta fragments typically produce craters only a few km in size. However, larger and/or faster fragments, such as might be produced by catastrophic disruption of a moon, might create bigger craters.

Finally, *Nearly Isotropic Comets* (NICs), which encompass long-period and Halley-type comets, are thought to originate in the Oort Cloud (Dones et al. 2004). The classical "outer" Oort Cloud is estimated to contain between 1×10^{11} and 3×10^{11} comets with $d > 1$ km (Francis 2005). Of these, roughly 10^8 comets are likely to be on Saturn-crossing orbits, assuming a cometary perihelion distribution which is flat or gradually increasing with distance from the Sun (Mazeeva 2007). However, because of their long orbital periods around the Sun and the limited degree of gravitational focusing by Saturn they undergo, impact rates due to NICs on Saturn's moons interior to Titan's orbit are probably one to two orders of magnitude smaller than the rate due to ecliptic comets (Zahnle et al. 1998, 2003). Because NICs encounter Saturn at higher speeds and therefore undergo less gravitational focusing, they become relatively less important for the moons closest to Saturn. By the same logic, cratering by NICs could be important for Iapetus and the irregular satellites, however.

19.3 Heavy Bombardments

Even before the Apollo landings, it was clear that crater densities on the lunar highlands were larger than could have been produced at present-day impact rates (Hartmann et al. 2000). Dating of lunar samples appeared to show that some basins, such as Imbrium, formed late, 3.8–3.9 Ga, i.e., some 700 Myr after the planets had formed. In a classic paper, Wetherill (1975) considered possible reservoirs of long-lived impactors, including accretional leftovers in the region of the terrestrial planets and Uranus-Neptune planetesimals (cf. Wetherill 1981). Bottke et al. (2007) dealt a blow to the idea of long-lived leftovers of terrestrial planet accretion. They showed that, even if an implausibly large mass of small bodies had been present soon after planet formation, collisional and dynamical evolution would have depleted the small bodies so severely that too few were left to make even a single basin as recently as 3.9 billion years ago.

In the past decade, Wetherill's ideas about long-lived Uranus-Neptune planetesimals have been combined with insights about dynamical chaos acting on long timescales (Sussman and Wisdom 1992; Laskar 1996; Thommes et al. 1999, 2002, 2008; Levison et al. 1998, 2001, 2004), culminating in the "Nice model".

The Nice model proposes that the orbits of the giant planets changed significantly long after the planets had formed (Tsiganis et al. 2005; Morbidelli et al. 2005; Gomes et al. 2005). In this picture, the four giant planets formed close together, between ∼5.5 and ∼14–17 AU of the Sun, compared with the present range of 5.2 to 30.1 AU. A massive (∼35 Earth mass) disk of planetesimals, i.e., a weighty ancestor of today's Kuiper Belt, is assumed to lie outside the planetary orbits. Some planetesimals near the inner edge of the disk, initially around 15 AU, evolve onto planet-crossing orbits, resulting in slow migration of the planets (Fernández and Ip 1984; Malhotra 1993; Murray et al. 1998; Hahn and Malhotra 1999; Gomes et al. 2004). In the simulations of the Nice model, slow migration continues for times ranging from 350 Myr to 1.1 Gyr, during which the disk loses about one-third of its mass. At this point, Jupiter and Saturn

cross the strong 1:2 mean-motion resonance. This event excites the eccentricities of Jupiter and Saturn's orbits, triggering an instability in the orbits of all the giant planets. The orbits of Uranus and Neptune become chaotic, causing them to suffer close encounters with each other and, in many cases, with Saturn. The ice giants are scattered onto eccentric orbits that traverse the planetesimal disk, thereby scattering bodies in the massive "Kuiper Belt" all over the Solar System. The planets' orbits are eventually circularized by dynamical friction exerted by the planetesimals (e.g., Del Popolo 2001; O'Brien et al. 2006; Leinhardt et al. 2009). In a few Myr, half the mass left in the disk prior to the resonance crossing is eliminated, and after some tens of Myr, 99% of the mass has been scattered out of the Solar System. During the chaotic phase, most main-belt asteroids would have become unstable as well due to sweeping resonances as the outer planets moved about. In the baseline model, the mass striking the Moon in comets would have been roughly comparable to the amount in asteroids (Gomes et al. 2005; Strom et al. 2005).

Depending upon the initial conditions, Jupiter and Saturn might have passed through a strong resonance other than the 1:2 as they migrated (Morbidelli et al. 2007). For our purposes, the key point is that it is quite plausible that the giant planets underwent a dynamical instability long after they formed. Independent of the details of what actually happened, it is plausible that there were profound implications for the saturnian satellites that were present at that time.

Whether or not the Nice model scenario actually happened remains unproven, although the model explains many features of the outer planets, most remarkably their semimajor axes, eccentricities, and mutual inclinations (Tsiganis et al. 2005), as well as other features such as the orbital distribution and mass of the jovian Trojans (Morbidelli et al. 2005) and the inclinations of neptunian Trojans (Lykawka et al. 2009). Other models for the LHB have been proposed, some of which would predominantly operate in the inner Solar System and have lesser effects on the saturnian satellites. While a bombardment of saturnian satellites roughly simultaneous with the inner Solar System LHB has been widely assumed, it has not been established. As we noted earlier and will see in Section 19.6, the current impact rate in the Saturn system by heliocentric bodies is insufficient to explain the apparently saturated populations of large craters on some of Saturn's moons, so the impact rate must have been higher at some point in the past. But whether it was the declining phase of early satellite accretion, due to one or more Solar System-wide or local impact spikes, or largely due to collisional evolution of satellites within the Saturn system cannot be securely assumed, despite the early post-Voyager assumptions. Nevertheless, at this time, the Nice model provides the most detailed Solar System-wide cratering chronology that is available.

19.4 Cratering Chronologies

A cratering chronology is a function that specifies the number of craters on a surface as a function of age. Three chronologies have been used in recent studies of cratering in the outer Solar System.

The *Neukum lunar chronology* has been used by Neukum and colleagues (Neukum et al. 2001). In Neukum's view, the same impactors (asteroids) have produced most of the primary craters on both the Moon and the satellites of Jupiter and Saturn, and so the rate at which bodies of diameter d strike the saturnian moons is taken to be proportional to the rate at which these bodies strike the Moon. The chronology is an updated version of that derived by the Basaltic Volcanism Study Project (1981 [Table 8.4.2, p. 1072]). Neukum (1983) fit the lunar data with a linear term, representing a constant cratering rate, plus an exponential term with an e-folding time of 144 Myr which dominates at early times. Marchi et al. (2009) use the same functional form, $N_1(t) = a(\exp(t/\tau) - 1) + ct$, where $N_1(t)$ represents the number of craters with diameter $D > 1$ km per km^2, t is the age of the terrain in Gyr, and a, τ, c are empirically derived constants. Marchi et al. (2009) find numerical values of $a = 1.23 \times 10^{-15}$, $\tau = 0.127$, and $c = 1.30 \times 10^{-3}$. The rate of crater formation per unit area, dN_1/dt, equals $a \exp(t/\tau)/\tau + c$. The exponential term exceeds the constant term for ages larger than 3.5 Gyr.

The Neukum model assumes that the flux of asteroids on any surface in the Solar System occurred with the same time dependence as measured for the Moon, and that the cratering record in the saturnian system stems from asteroids captured into planetocentric orbits about Saturn, not simply asteroids moving on heliocentric, Saturn-crossing orbits. The planetocentric aspect of this chronology is strongly, but not entirely, driven by a perceived need to explain the lack of strong apex-antapex cratering asymmetries in the outer Solar System. We discuss the apex-antapex issue in Section 19.6, and return to the issue of asteroid capture in Section 19.8. To calibrate the lunar chronology at Saturn, Neukum assumes that the oldest surface on Iapetus is 4.4 Ga (Castillo-Rogez et al. 2007). Chronologies for other saturnian satellites are derived by scaling from Iapetus' record, assuming that the impactors orbit Saturn with eccentricities of 0.6 and inclinations of 15° (Horedt and Neukum 1984b). The Neukum model assumes captured asteroids as the main source of impactors, but allows comets to play some role during recent epochs.

The *cometary chronology* uses estimates of the numbers of "comets" of different sizes crossing Saturn's orbit at the present epoch to calculate cratering rates (Smith et al. 1981, 1982; Shoemaker and Wolfe 1981, 1982). The cratering rate dN/dt is assumed either to be constant with time (a reasonable approximation for at least the last three billion

years) or to have monotonically decreased with time. For example, based on the work of Holman and Wisdom (1993), Zahnle et al. (1998, 2003) assumed that the population of bodies crossing the orbits of the giant planets has declined inversely with time since the Solar System formed, i.e., dN/dt $\propto (t_0–t)^{-1}$, where $t_0 = 4.567$ Gyr. With this assumption, the crater density on a surface of age t is proportional to $\ln [t_0/ (t_0–t)]$. The cometary chronology is primarily intended for application to young surfaces. It takes the view that N(t) is unknown for the outer Solar System, since the impacting population (comets) differs from that of the Moon (asteroids), and there are no radiometrically dated surfaces on the satellites of the giant planets. Zahnle et al. (2003) computed the cometary chronology for satellites of the giant planets under two assumptions about the impactors' size distribution: "Case A," based upon the paucity of small primary impact craters on the galilean satellites (Bierhaus et al. 2005), and thus poor in small comets; and "Case B," based on high-resolution crater counts on Triton (McKinnon et al. 2000) and richer in small comets. Because of the much larger abundance of small comets in Case B, a given crater density translates into a younger age in Case B.

The *Nice model chronology* assumes that most of the impacts on the regular satellites of the giant planets took place around the time of the dynamical instability in the model. The Nice model cannot predict exactly when the resonance crossing took place, but 700 Myr after the formation of the giant planets (i.e., 3.9 billion years ago) lies within the range found in the simulations. Gomes et al. (2005) assumed that the lunar LHB 3.9 Ga was caused by the flood of outer Solar System planetesimals and asteroids released by the instability. If that assumption is correct, the Nice model provides the basis for a Solar System-wide chronology, although "comets" (which, on average, bombard planetary surfaces somewhat earlier than asteroids) produce almost all the impacts on bodies in the outer Solar System, while both asteroids and comets contribute on the terrestrial planets and their satellites. Charnoz et al. (2009) applied the Nice model chronology to the origin of Saturn's rings, calibrating the model by the observed density of basins and 10-km craters on Iapetus, and found that the rings could have formed at that time by disruption of a satellite at the current location of the rings.

19.5 Impact Physics and Scaling Laws

The size-frequency distribution of craters on the surface of a planetary body is not a faithful reflection of the size-frequency distribution of the hypervelocity impactors that create them. Because the final craters are typically at least 10 times larger in diameter than the object that strikes the surface, the final crater diameter distribution may present a distorted picture of the impactor population. Factors such as the porosity of the surface (an extreme factor in the case of Hyperion), varying impact velocity, and impact angle all contribute to differences between the populations of craters and impactors. The same parent population of projectiles may produce radically different crater size-frequency distributions on different satellites, especially when considered in an absolute sense. It is thus critical to understand the relation between the diameter of the final crater and the impacting projectile and its dependence on the various conditions of impact.

Because we are as yet unable to perform direct experiments with kilometer-size projectiles impacting full-scale planetary targets, we must rely on so-called scaling relations that relate the results of small-scale experiments and numerical simulations to actual craters in the Solar System. Refined by many investigators over many decades of work, such scaling relations now give reasonably reliable results. They are no longer wholly empirical: physics-based numerical simulations have recently achieved great success in both reproducing the results of small-scale laboratory and field experiments[5] and justifying the empirical extrapolations of the past.

Employing the highly successful methods long established in fluid mechanics, crater scaling is based on relations between dimensionless combinations of variables describing the properties of the projectile and target, often expressed in the language of the Buckingham Π theorem (Buckingham 1914). The most important groups are the cratering efficiency, described as the ratio of either the crater diameter to the projectile diameter or the ratio of crater volume to projectile volume, and the inverse Froude number that expresses the ratio between gravitational forces and inertial forces. In all cases the crater diameter or volume pertains to the "transient crater", which is formed immediately after the impact. In nearly all planetary circumstances the transient crater subsequently collapses and expands in diameter (while it shrinks in volume) to produce the final, observed, crater. We thus also need a relation between the transient crater and final crater before we can link the impactor population to that of the observed craters.

The cratering efficiency is defined as either π_V or π_D, depending on whether the transient crater volume or diameter is more convenient. These definitions also traditionally incorporate the ratio between the projectile and target densities in the following forms:

$$\pi_V = \frac{\rho V}{m} \tag{19.1a}$$

[5] Field experiments here refer to explosion cratering tests, and to laboratory impact experiments performed at elevated gravity in a centrifuge, which simulate similar scales (e.g., Schmidt and Housen 1987).

and

$$\pi_D = D_t \left(\frac{\rho}{m}\right)^{1/3} \tag{19.1b}$$

where V is the excavated volume of the crater, D_t is the transient crater diameter, ρ is the density of the target, and m is the mass of the projectile. The inverse Froude number, or "gravity-scaled size," is usually expressed as:

$$\pi_2 = \frac{3.22ga}{U^2} \tag{19.2}$$

where U is the speed of the impact, g is the surface gravity of the target and a is the mean radius of the projectile.[6] The relation between the cratering efficiency and the gravity scaled size closely approximates a power law (Holsapple 1993, 2009). The exponents of this power law depend on whether the crater size is more dependent upon the momentum or the energy of the impactor, a dependence that is a function of the dynamics of the impact and which cannot be determined from the scaling relations alone.

Thus, we can write

$$\pi_V \propto \pi_2^{-3\mu/(2+\mu)} \left(\frac{\rho}{\delta}\right)^{(2+\mu-6\nu)/(2+\mu)} \tag{19.3}$$

where δ is the density of the impactor and μ and ν are experimentally determined constants (e.g., Melosh 1989; Holsapple 1993, 2009). The case when $\mu = 1/3$ corresponds to "momentum scaling" (i.e., the crater's volume depends on the momentum of the impactor, independent of its velocity), while $\mu = 2/3$ gives "energy scaling" (the crater's volume depends on the energy of the impactor, independent of its velocity) (Holsapple and Schmidt 1982).

These relations are frequently expressed by the simpler relations for practical use:

$$\pi_V = C_V \pi_2^{-\alpha} \tag{19.4a}$$

$$\pi_D = C_D \pi_2^{-\beta} \tag{19.4b}$$

where C_V, C_D, α, and β are dimensionless constants that are either determined empirically or from computer simulations. For impacts into competent rock (or ice) or water-saturated soil these constants are given by $C_V = 0.2$, $C_D = 1.6$, $\alpha = 0.65$, and $\beta = 0.22$.

There may be other dimensionless constants in the problem. For example, it is well known that the cratering efficiency for sand is substantially smaller than that for competent rock; for sand $C_V = 0.24$, $C_D = 1.68$, $\alpha = 0.51$, and $\beta = 0.17$ may be used (cf. Table 1 in Holsapple [1993] and Table 7.1 in Melosh [1989]). Craters on the highly porous satellite Hyperion, therefore, should not follow the same scaling relations as craters on more densely compacted icy satellites. (Cratering in porous bodies has been studied experimentally [Housen and Holsapple 2003], but impact simulations involving porosity are only now becoming possible [Jutzi et al. 2008, 2009; Leinhardt and Stewart 2009]). So-called sand or dry soil scaling probably also applies to saturnian satellites of more modest porosity (such as Phoebe; Giese et al. 2006) and to craters formed in the regoliths and megaregoliths of highly battered midsize satellites such as Rhea and Iapetus. Until recently, it was not possible to disentangle the independent effects of porosity and internal friction on cratering efficiency because these two factors are closely linked for all materials on which experiments have been performed to date. However, recent numerical work (Wünneman et al. 2006, 2008) using a newly formulated model for introducing porosity into hydrocode computations has evaluated these factors separately and finds both to be about equally important.

The angle of impact is also an important factor whose effect on cratering efficiency has been poorly understood. A commonly used *ansatz* has been to replace U in the above scaling relations with the vertical component of velocity, U sin θ, where θ is the angle between the trajectory of the impactor and the plane of the target surface (e.g., Chapman and McKinnon 1986). This *ansatz* has recently received strong support from 3-dimensional hydrocode simulations (Collins et al. 2009) for dense targets, but it remains to be verified for porous targets.

The diameter of a simple crater, D_s, is somewhat larger than the diameter of the transient crater, D_t, because even simple craters suffer some degree of rim collapse after they form (Melosh 1989). For the purposes of this paper, we relate the simple crater diameter D_s, measured in km, to the impactor diameter d through

$$D_s = 11.9 \left(U^2/g\right)^{0.217} (\delta/\rho)^{0.333} (d/\mathrm{km})^{0.783} \tag{19.5}$$

with U in km/s and g in cm/s^2, and "final" diameter D in km given by

$$D = D_s \text{ for } D_s < D_c \tag{19.6a}$$

$$D = D_s (D_s/D_c)^{\xi} \text{ for } D_s > D_c \tag{19.6b}$$

where D_c is the transition diameter from the simple to collapsed, complex morphology. Equation 19.5 is derived from Eq. 19.4b with competent rock parameters (see Zahnle et al. 2003); Holsapple (2009) states that these parameters are also appropriate for cold ice. In this paper we take $D_c = 2.5$ km for Titan and $D_c = 15$ km for Saturn's other satellites (Schenk 1989; Schenk et al. 2004). We take $\xi = 0.13$

[6] The factor $3.22 = 2\sqrt[3]{4\pi/3}$ reflects historical inheritance from explosion cratering studies, and is not of any fundamental physical significance.

(McKinnon et al. 1991). We assume an impactor density of $\delta = 0.6\,\mathrm{g/cm^3}$, consistent with the density of the nucleus of Comet Shoemaker-Levy 9 (Asphaug and Benz 1996, and see Sosa and Fernández 2009 for density estimates for ten periodic comets). Eqs. 19.5 and 19.6 represent a compromise between unwarranted precision and practicality, though we recognize that accurate simple-to-complex transition diameters can now be derived for the mid-sized saturnian satellites from Cassini images, and on theoretical grounds are expected to vary according to satellite gravity (e.g., McKinnon 2007)[7]. The reader can experiment with various scaling relations using the interactive calculators provided by Melosh and Beyer (2009) and Holsapple (2009).

Typical impact velocities are given by

$$U_{mean} = \left(3{v_{orb}}^2 + {v_\infty}^2 + {v_{esc}}^2\right)^{1/2} \tag{19.7}$$

where v_{orb} is the orbital speed of the satellite around Saturn, v_∞ is the velocity at "infinity" of the body encountering the Saturn system, and v_{esc} is the escape velocity from the surface of the satellite (Lissauer et al. 1988; Zahnle et al. 2003). The final term is negligible for our purposes, so we will neglect it henceforth. The minimum and maximum impact speeds are approximately

$$U_{slow} = \left(2{v_{orb}}^2 + {v_\infty}^2\right)^{1/2} - v_{orb} \tag{19.8a}$$

and

$$U_{fast} = \left(2{v_{orb}}^2 + {v_\infty}^2\right)^{1/2} + v_{orb} \tag{19.8b}$$

respectively.

In Fig. 19.3, we use Eqs. 19.5 and 19.6 to plot the diameter (d) of the cometary impactor (vertical axis) needed to make a crater of diameter D on Mimas, Rhea, and Iapetus. The assumed impact speeds on Mimas are 6.2 ("slow"), 25.0 ("mean"), and 34.8 km s^{-1} ("fast"); for Rhea, 3.9, 15.0, and 20.9 km s^{-1}; and for Iapetus, 2.2, 6.4, and 8.8 km s^{-1}. Ten-km craters on Mimas are made by fast impactors with diameters of only 0.2 km, 0.3 km at the mean impact speed, and 0.6 km for slow impactors. For Rhea, the corresponding impactor sizes are 0.4, 0.5, and 1.1 km, respectively; for Iapetus, 0.7, 0.8, and 1.4 km. Three-hundred-km craters, i.e., basins, are made by 11-, 13-, and 26-km-diameter impactors at Mimas; 22-, 26-, and 55-km-diameter impactors at Rhea; and 33-, 40-, and 71-km-diameter impactors at Iapetus, again, all at the impact speeds given above, respectively. If we wish to tie the cratering record of the satellites to the

[7] The scaling exponent $\xi = 0.13$ was derived from the depth-diameter relations for lunar craters assuming volume conservation during collapse. The value of this exponent should be reassessed for the mid-sized icy satellites.

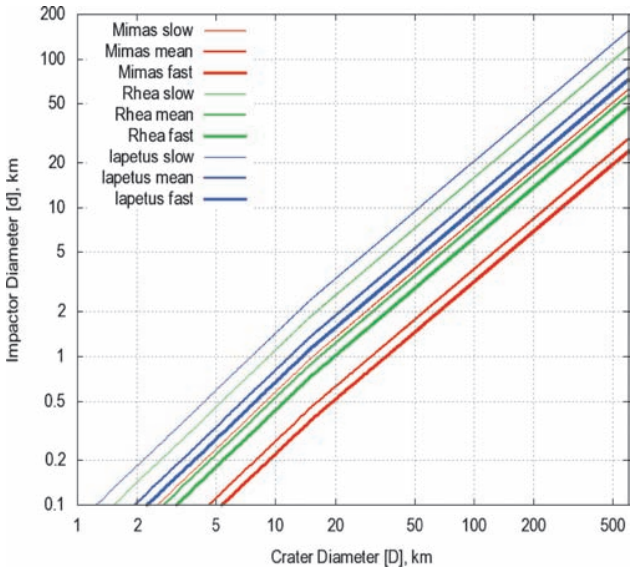

Fig. 19.3 Impactor diameter d (*vertical axis*) required to produce a crater of diameter D (*horizontal axis*) on Mimas, Rhea, and Iapetus. We use Eqs. 19.2 and 19.3 with the following parameters: $\rho_i = 0.6$; $\rho_t = 0.9$ (all three moons are assumed to have icy shells); U given by Eqs. 19.4–19.6 with $v_{orb} = 14.32$, 8.49, and 3.27 for Mimas, Rhea, and Iapetus, respectively; $v_\infty = 3$; $g = 6.36$, 26.4, and 22.3; $Dc = 15$; and $\xi = 0.13$

putative impactors from the swarm of ecliptic comets, basins on Iapetus, Titan, and Rhea are our best bets, because the required impactor sizes overlap the size range for which we know a bit about the Kuiper Belt size-frequency distribution, and for which we have some constraint on absolute numbers and rates (e.g., Fuentes et al. 2009).

19.6 Predicted Cratering Rates by Comets

Heliocentric (Sun-orbiting) "comets" on Saturn-crossing orbits, which roam the outer Solar System in numbers too big to ignore, are the only present-day *known* population of potential impactors for Saturn's inner moons. The cometary population can be characterized by astronomical observations, both current and historical, the observed orbital distribution can be corrected for discovery biases, and their statistical impact probabilities can be computed. Such astronomically based impact rates have been used to estimate the ages of young and middle-aged surfaces on the satellites of the outer planets (Zahnle et al. 2003). We will review this line of reasoning here.

On the other hand, there is evidence that many or perhaps most of the craters in the Saturn system may be of planetocentric (Saturn-orbiting) origin. The key issues are the global uniformity of cratering and the large abundance of small craters. Heliocentric origin strongly favors cratering of

the leading hemisphere of synchronously rotating satellites (Shoemaker and Wolfe 1982; Horedt and Neukum 1984a; Zahnle et al. 2001), while planetocentric cratering weakly favors the leading or trailing side, depending on whether the debris fall from outside or inside the satellite's orbit, respectively (Horedt and Neukum 1984a, Alvarellos et al. 2005). Cratering asymmetries due to captured irregular satellites would likewise depend on whether the irregulars were prograde or retrograde. Strong apex-antapex asymmetries have not been detected on any satellite in the outer Solar System, except for the perverse case of Neptune's moon Triton (Schenk and Zahnle 2007). The origin of voluminous planetocentric debris is often attributed to a cataclysm or cataclysms, possibly linked to the destruction of a moon or the formation of the rings or both (Smith et al. 1981, 1982; Chapman and McKinnon 1986; Lissauer et al. 1988). If planetocentric cratering has been dominant, the surfaces are younger than we have inferred by assuming that the impactors come from heliocentric orbit. If there has been a geologically *recent* cataclysm, such as the post-Voyager idea that Saturn's rings formed within the last 100 Myr (Esposito 1986; cf. Lissauer et al. 1988; Dones 1991; Charnoz et al. 2009; and Chapter 17), we can use heliocentric impact rates to estimate the probability of such an event, but not precisely when it occurred.

As we discussed in the Introduction, Population I and Population II craters were generally taken by Voyager-era scientists to be made by heliocentric and planetocentric bodies, respectively. The craters themselves can be called "primary" and "sesquinary" (formerly "poltorary"; Dobrovolskis and Lissauer 2004), respectively, to distinguish them from conventional secondaries that fall back to the cratered satellite immediately (Zahnle et al. 2008). In one picture Population I is (or was) responsible for the larger craters, while Population II is responsible for most of the small craters.

More recent observations support the importance of both heliocentric and planetocentric impactors on the satellites of the giant planets, but unequally. The Galileo spacecraft returned images of Ganymede and Europa that show remarkably few small (1-to-20 km diameter) *primary* impact craters on young surfaces (Bierhaus et al. 2001; Schenk et al. 2004; Bierhaus et al. 2005; McEwen and Bierhaus 2006), but numerous secondaries. On the other hand, Triton has a young surface with a "typical" size-frequency distribution of small craters. But on retrograde Triton, the leading-trailing asymmetry is so extreme that it is not clear whether we are seeing the results of heliocentric comets or head-on collisions with prograde planetocentric debris (Croft et al. 1995; Schenk and Sobieszczyk 1999; Stern and McKinnon 2000; Schenk and Zahnle 2007).

Here we focus on heliocentric comets and primary craters. We take the chief source of primary craters in the outer Solar System to be the ecliptic comets [ECs] (Shoemaker and Wolfe 1982; Smith et al. 1982, 1986, 1989; Zahnle et al. 1998, 2003; Levison et al. 2000; Schenk et al. 2004). ECs refer to low inclination, prograde comets that interact strongly with planets: Jupiter-family comets, Centaurs, and Scattered Disk Objects. Long-period comets (also known as Oort Cloud comets) and Halley-type comets, even when lumped together as "Nearly Isotropic Comets" (NICs; Levison 1996), are important at Saturn (at the ∼10%–30% level) only for Iapetus and the irregular satellites (see Section 19.2). The distinct inclination distributions of the ecliptic comets and the nearly isotropic comets suggest that they arise from different reservoirs, with the former evolving inward from the Kuiper Belt/Scattered Disk, while the latter fall from the Oort Cloud (Duncan et al. 1988; Levison and Duncan 1997; Gladman et al. 2001; Dones et al. 2004).

To compute cratering rates, we have two types of information. The modern cratering rate can be estimated by characterizing the current populations of impacting bodies (comets), calculating impact probabilities, and using scaling rules to estimate the sizes of the resulting craters (see Section 19.5). A time-averaged ("historical") cratering rate can be estimated from the numbers of craters and basins observed on unsaturated satellite terrains (Zahnle et al. 2003; Kirchoff and Schenk 2009b). The major uncertainties are the age of the surface and the constancy of the impact rate. In practice the only usable date is the 3.9 Gyr age of the LHB, which is sensibly explained in the Nice model as a Solar System-spanning feature caused by a rearrangement of planetary orbits (Section 19.3; Morbidelli et al. 2007; Levison et al. 2008). We can take the cratering rate as constant, or we can impose the inverse-time decay relation suggested by numerical integrations (Holman and Wisdom 1993; see Dobrovolskis et al. 2007 for a more general discussion of impact rate decay curves). During the era of heavy bombardment effects on satellite surfaces may have been especially severe; such effects include saturation cratering, complete disruption, and surface melting (Chapman and McKinnon 1986; Levison et al. 2001; Barr and Canup 2008). Whatever the source or sources of the heavy bombardment on the saturnian satellites, the historical rates refer to the time since the heavy bombardment ended.

Arguably, the best source for historical crater counts in the outer Solar System is Ganymede's younger (bright) terrains. These terrains have been geologically reworked since the LHB. The upper bound age of ∼3.9 Gyr and a constant impact rate imply that Jupiter has been struck 2×10^{-3} per year by cometary nuclei with diameters $d \geq 2$ km, which corresponds to 8×10^{-4} per year striking Saturn, using the ratio of 42 Saturn impacts to 100 Jupiter impacts calculated by Levison and Duncan (1997). The characteristic time scale set by the orbital rearrangement in the Nice model is ∼10 Myr (Gomes et al. 2005). The $dN/dt \propto (t_0–t)^{-1}$ decay law then implies that the current impact rate is smaller than the

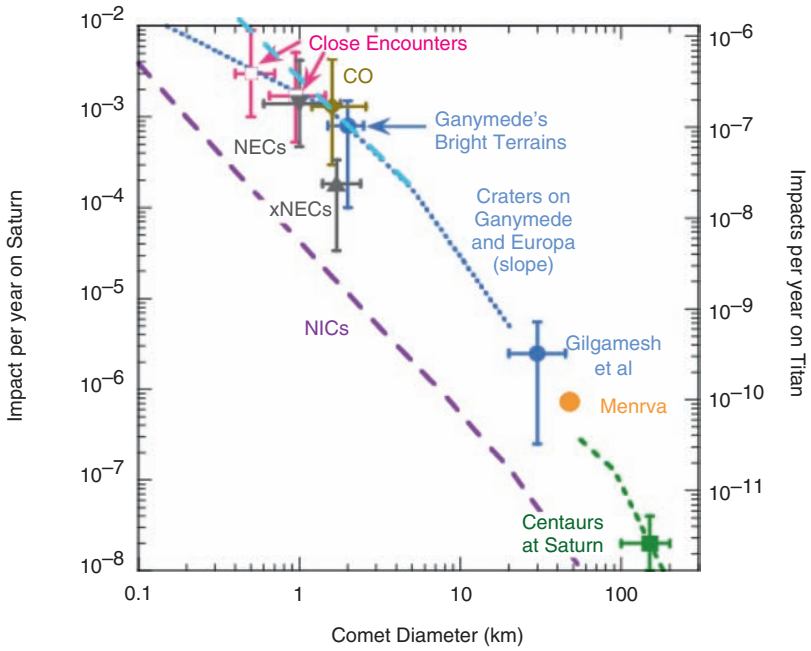

Fig. 19.4 Impact rates at Saturn and Titan. "Close Encounters" is deduced from the historical record of comets known to have passed near Jupiter. "CO" refers to the impact rate that would be deduced if excess carbon monoxide in Jupiter's stratosphere had been caused by comet impact. Points labeled "NECs" and "xNECs" refer to impact rates computed from the roster of known Jupiter-family comets by Levison et al. (2000) and Bottke et al. (2002), respectively. Points labeled "Ganymede" and "Gilgamesh" are impact rates inferred from impact craters on Ganymede and Callisto. Titan's 440-km basin Menrva (Lorenz et al. 2007) is conservatively taken to represent a once in 10 Gyr event. The associated lines are deduced from the size-frequency distributions of craters on Europa and Ganymede. The point labeled "Centaurs" refers to the three big Centaurs currently known to be on Saturn-crossing orbits. The line through "Centaurs" is based on the observed populations of Kuiper Belt Objects. The dashed line refers to impacts by long period and Halley-type comets ("NICs"). Case A (blue dots) refers to the relative abundance of small comets at Europa and Ganymede, while Case B (blue dashes) refers to the relative abundance of small impacting objects at Triton

long term average by a factor ln(3.9 Gyr/10 Myr) ~6.[8] The corresponding current impact rate on Saturn of $d \geq 2$ km comets would be 1×10^{-4} per year. Since the bright terrains might be considerably younger than 4 Gyr, we plot this point (in light blue) in Fig. 19.4 at 8 $(+16, -7) \times 10^{-4}$ year^{-1} at $d = 2.0 \pm 0.5$ km. If geological reworking of Ganymede took place independently of the great rearrangement in the Nice model (or other heavy bombardment), a relatively high impact rate is appropriate.

There are four (possibly five) big, young impact basins on Ganymede and Callisto, with Gilgamesh and Valhalla being the best-known (e.g., Schenk and McKinnon 2008). These basins were made by comets with $d \geq 30 \pm 10$ km. Spread uniformly over 4 Gyr, these four impacts imply an impact rate of 30 km comets on Saturn of dN/dt $(d \geq 30 \pm 10\,\text{km}) = 2.5\,(+3, -2) \times 10^{-6}$ year^{-1}. As above, the $(t_0\text{–}t)^{-1}$ decay implies current impact rates that are 6 times smaller.

The current population of ecliptic comets can be inferred from any of (a) the number of small comets observed near the Earth; (b) the historical record of small comets known to have closely encountered Jupiter[9]; or (c) the observed number of Centaurs in the more distant Solar System.

Levison and Duncan (1997) modeled the evolution of test particles from sources in the Kuiper Belt. In modeling the migration of ecliptic comets, Levison and Duncan assumed a dynamically cold (low inclination, low eccentricity) classical Kuiper Belt source. Levison and Duncan calibrated their model to the number and orbital properties of JFCs that reach deep into the inner Solar System. Levison et al. (2000) developed this to estimate an impact rate at Saturn dN/dt $(d > 1\,\text{km}) = 1.4 \times 10^{-3}$ year^{-1}, with a quoted uncertainty of "at least an order of magnitude." This point is plotted on Fig. 19.4 as "NECs," which

[8] t_o here refers to initiation of the LHB, e.g., when Jupiter and Saturn cross their 1:2 mean-motion resonance.

[9] Because of the steep decline in reflected brightness with distance from the Sun for small bodies, the census of Saturn-crossing comets is vastly inferior to that of JFCs. Lagerkvist et al. (2000) and Hahn et al. (2006) have identified three ecliptic comets that have passed within 0.01 and 0.03 AU of Saturn, i.e., roughly at Iapetus' distance from the planet. Nevertheless, this represents a vast improvement with respect to the Voyager era, when Shoemaker and Wolfe (1982) of necessity based their bombardment rates on the observations of single bodies (e.g., asteroid/extinct comet Hidalgo, or Chiron).

stands for "Near-Earth Comets". Bottke et al. (2002) updated the arguments of Levison et al. (2000) by using observations of inactive comets obtained from their analysis of discovery rates in the Spacewatch Near-Earth Object survey. From six objects Bottke et al. deduce that there are currently 61 ± 50 dormant JFCs with $d > 1.7$ (+0.7, –0.3) km, for which the corresponding impact rate on Saturn would be dN/dt ($d > 1.7$ [+0.7, –0.3] km) $= (1.8 \pm 1.4) \times 10^{-4}$ year^{-1}. This point is plotted on Fig. 19.4 as "xNECs".

An independent approach exploits the historical record of comets observed to have made close approaches to Jupiter. As reviewed by Schenk and Zahnle (2007), observers have recorded four close approaches within 3 Jupiter radii and two direct hits since the dawn of the telescopic era. A lower bound on the sizes of these six is $d > 1.0$ (+0.5, –0.3) km. Six encounters inside of 4 Jupiter radii over 350 years implies an impact rate on Jupiter of at least 4×10^{-3} year^{-1}, corresponding to 1.7×10^{-3} year^{-1} on Saturn[10]. Another source of information is more recent comets making more distant encounters. Observations and orbital simulations indicate that at least 9 comets crossed Callisto's orbit between 1950 and 1999 (a sample that we have some hope might be complete). The smallest of these has a diameter of $d \sim 0.5$ km (Lamy et al. 2004). The corresponding impact rate on Saturn would be $3 \cdot 10^{-3}$ year^{-1} for $d > 0.5$ km. Another independent argument uses excess CO present in Jupiter's stratosphere to infer the recent impact history (Bézard et al. 2002; also see Lellouch et al. 2005 for a possible similar event on Neptune). Excess CO is removed by mixing into the troposphere over ~300 years. The impact of Shoemaker-Levy 9 (SL9) produced $\sim 7 \times 10^{14}$ g of CO (Lellouch et al. 1997) from a $\sim 10^{15}$ g comet (Harrington et al. 2004), but this falls well short both in quantity and location of being able to account for all the excess CO in the jovian stratosphere; the old CO suggests that another comet as big or bigger than SL9 has hit Jupiter in the past 300 years. The point is plotted on Fig. 19.4 as "CO".

We would like to estimate the impact rate on Saturn from the numbers and characteristics of Saturn-crossing ecliptic comets. For very big Saturn-crossing Centaurs, discovery may be nearly complete. The problem is that they require a huge extrapolation of the size-frequency curve to scale them to the desired quantity, the number of small Centaurs, because counts of smaller Centaurs and Saturn-crossing comets are severely incomplete. Here we will use the three known large Centaurs on Saturn-crossing orbits: Chiron, Pholus, and 1995 SN_{55} (the latter unnamed and unnumbered because it is lost). All appear to be roughly 150 km diameter, with absolute magnitudes, H, in the range 6–7 (Fernández et al. 2002; Groussin et al. 2004; JPL Solar System Dynamics Small-Body Database Browser 2009). Their annual statistical ("Öpik") impact probabilities with Saturn are 1.5×10^{-8}, 1.0×10^{-9}, and 3.5×10^{-9}, respectively (though, naturally, the orbital elements upon which such probabilities are based vary strongly on million-year time scales for these and all Saturn-crossing Centaurs, and are especially uncertain for 1995 SN_{55}; Horner et al. 2004). Added together, they imply that $d = 150 \pm 50$ km objects hit Saturn at a rate of $2\,(+2, -1) \times 10^{-8}$ year^{-1}.

To extend this datum to smaller sizes requires a size distribution. Size-frequency distributions have been determined for Kuiper Belt Objects, but these are not yet trustworthy for diameters smaller than 50 km (see the review of Petit et al. 2008), while the sizes of the bodies that crater satellites range from <1 km (for 20 km craters on the moons interior to Dione; see Table 1 of Zahnle et al. 2003) to ~70 km for Iapetus' ~580-km basin Turgis (Giese et al. 2008; Kirchoff and Schenk 2009b; USGS Astrogeology Gazetteer of Planetary Nomenclature 2009; see Section 19.5). An SFD with a power-law index $a = 4$–5 now seems well established for KBOs larger than a few tens of km in diameter (Petit et al. 2008)[11]. More recently, Fuentes et al. (2009) report *differential* SFDs with power-law indices of 4.65 (+0.4, –0.45) for $d > 90 \pm 30$ km, with a sharp knee, with an index of 2.0 (+0.6, –0.7) for $d < 90$ km (see Fig. 19.1). Because the smallest bodies that have been detected in the shallow, small-size end of the distribution are tens of km in diameter, there is little information for bodies with $d < 50$ km.

From crater counts on Ganymede, Zahnle et al. (2003) inferred effective slopes of the cumulative impactor size distribution of $b = 1.7$ for 2 km $< d <$ 5 km and $b = 2.5$ for 5 km $< d <$ 20 km. Jupiter's Trojan asteroids provide another sample of quasi-local debris at sizes that can bridge the gap, assuming no collisional evolution within each cloud. (In the Nice model, Jupiter's Trojans are captured from the same outer Solar System population that gave rise to today's Kuiper Belt [Morbidelli et al. 2005, 2009], so the link is genetic.) Szabó et al. (2007) find $b = 2.2 \pm 0.25$ for absolute magnitudes between 9 and 13.5, which respectively correspond to diameters of 110 and 13 km, respectively, assuming a 4% albedo. For specificity we will use here a single $b = 2.5$ cumulative slope for 5 km $< d <$ 120 km and $b = 1.7$ for 1.5 km $< d <$ 5 km.

For small craters we use populations on Europa and those superposed on the young large basins Gilgamesh (on Ganymede) and Lofn (on Callisto). We invert the crater

[10] The extrapolated impact rate of $(3 \pm 2) \times 10^{-2}$ year^{-1} for impacts on Jupiter for $d > 0.3$ km is consistent with the July 2009 impact on Jupiter, which appears to have had an energy comparable to that of the smaller fragments of SL9 such as W.

[11] A differential distribution $dN/dD \propto D^{-a}$ is said to have a power-law index of a; the corresponding cumulative distribution would have a power-law index $b = a - 1$.

counts using Eqs. 19.5 and 19.6 to obtain the size-frequency distribution (SFD) of small comets at Jupiter. The inversions are shown in Fig. 19.4. Based on 150 estimated Europan craters with D > 1 km (Schenk et al. 2004), we infer a cumulative cometary SFD $N(>d) \propto d^{-b}$ with b = 0.9 for d < 1 km. From craters on Gilgamesh, the inferred slope of the power law distribution is b∼1.2 for d < 2 km.

The shallow size distribution we adopt for cometary nuclei with diameters between about 1 and 10 km is similar to size distributions of JFCs inferred from (some) observational studies, which are reviewed by Lamy et al. (2004). For example, Fernández and Morbidelli (2006) derive a value of b = 1.25 for faint JFCs with perihelion distances <1.3 AU. Size determinations of cometary nuclei are not easy, because the nucleus is unresolved in Earth-based telescopic images, and thus requires either careful subtraction of comae, or dubious empirical relationships between total cometary brightness and the size of the nucleus (the former technique is now much preferred, and is reasonably well-calibrated for HST images). In any case, the apparent progressive steepening of the cometary SFD at larger sizes has been suggested before (e.g., Weissman and Levison 1997). However, models of the formation and collisional evolution of Kuiper Belt Objects (Kenyon et al. 2008) do not yet match the size distribution inferred from the variety of observations we have described (Petit et al. 2008).

With these admittedly provisional, but constrained, limits on the cometary SFD and impact rates (Fig. 19.4), we consider the implications for Saturn's satellites. We consider two cases. In Case A, the mass distribution of small comets is consistent with what we find at Jupiter and on its satellites. Case A requires an additional source of (presumably) planetocentric debris to account for most small craters at Saturn (in that the relative flatness of the predicted crater SFD at smaller sizes is hard to reconcile with observations; see next section). In Case B, we use a mass distribution of small comets that would be consistent with small craters on Triton, which is steeper at smaller sizes. Case B may or may not require planetocentric debris to account for small craters. The results are given in Table 19.1.

For comparison, cratering rates at Saturn were estimated by Smith et al. (1982) and Lissauer et al. 1988). These studies predate the discovery of the Kuiper Belt, and so underestimate heliocentric impact rates and correspondingly overestimate cratering time scales and crater retention ages, typically by roughly an order of magnitude.

Finally, we find the Nearly Isotropic Comets (NICs) to be relatively unimportant for cratering at Saturn, given the number of such comets on Saturn-crossing orbits estimated earlier. these. We use the scalings discussed by Zahnle et al. (2003) to estimate the total impact rate by NICs (Table 19.1). Because NICs tend to strike at higher velocity than ECs, especially for the more distant moons, they contribute somewhat more to the cratering record there, but are relatively less important as one moves inward toward Saturn due to their limited gravitational focusing. Among the moons of Saturn listed in Table 19.1, NICs are most important for Iapetus, where they contribute 10% of the craters, and for Phoebe, where they contribute 30% of the impact craters due to comets. They only contribute at the 1% level at Dione.

19.6.1 Implications for Catastrophic Disruption

It has been suggested that a satellite breaks up if the predicted transient crater diameter exceeds the satellite's diameter

Table 19.1 Present-day cratering rates at Saturn

	Cratering rates				Cratering times	
	$\dot{C}_A(>10)$	$\dot{C}_B(>10)$	$\dot{C}_S(>10)$	$\dot{C}_{NIC}(>10)$	τ_A	τ_B
Mimas	$5.6 \cdot 10^{-14}$	$5.0 \cdot 10^{-13}$	$1.6 \cdot 10^{-14}$	$5.6 \cdot 10^{-16}$	80	17
Enceladus	$3.7 \cdot 10^{-14}$	$2.8 \cdot 10^{-13}$	$1.0 \cdot 10^{-14}$	$4.2 \cdot 10^{-16}$	80	19
Tethys	$2.6 \cdot 10^{-14}$	$1.8 \cdot 10^{-13}$	$4.3 \cdot 10^{-15}$	$2.8 \cdot 10^{-16}$	25	6.5
Dione	$1.7 \cdot 10^{-14}$	$1.0 \cdot 10^{-13}$	$2.7 \cdot 10^{-15}$	$2.2 \cdot 10^{-16}$	34	10
Rhea	$1.1 \cdot 10^{-14}$	$6.2 \cdot 10^{-13}$	$1.5 \cdot 10^{-15}$	$1.6 \cdot 10^{-16}$	29	9
Titan	$3.4 \cdot 10^{-15}$	$1.4 \cdot 10^{-14}$	$1.3 \cdot 10^{-15}$	$9.0 \cdot 10^{-17}$	9	4
Hyperion	$7.0 \cdot 10^{-14}$	$6.2 \cdot 10^{-14}$	$1.8 \cdot 10^{-15}$	$2.3 \cdot 10^{-16}$	1,400	300
Iapetus	$1.1 \cdot 10^{-15}$	$4.2 \cdot 10^{-15}$	$7.9 \cdot 10^{-16}$	$1.1 \cdot 10^{-16}$	380	180
Phoebe	$3.4 \cdot 10^{-16}$	$1.4 \cdot 10^{-15}$	$1.3 \cdot 10^{-15}$	$1.2 \cdot 10^{-16}$	54,000	2,400

These are calibrated to a Saturn impact rate of 0.0012 cometary nuclei with d > 1.5 km per year. Quoted cratering rates should be regarded as uncertain to a factor of 4. The rates given here are typically 0.6 times the rates given in Table 19.4 of Zahnle et al. (2003), primarily because we have adopted a slightly smaller cometary impact rate with Saturn than in Zahnle et al. (2003). The rates given for Titan apply to a body with Titan's mass and size, but without an atmosphere.
$\dot{C}_A(>10)$: Case A cratering rate D > 10 km[km^{-2} year^{-1}].
$\dot{C}_B(>10)$: Case B cratering rate D > 10 km[km^{-2} year^{-1}].
$\dot{C}_S(>10)$: Smith et al. (1982) cratering rates, D > 10 km[km^{-2} year^{-1}].
$\dot{C}_{NIC}(>10)$: NIC (=Halley-type + Long-period comet) cratering rate D > 10 km[km^{-2} year^{-1}].
τ_A: Case A timescale for D > 20 km craters [Myr].
τ_B: Case B timescale for D > 20 km craters [Myr].

(e.g., Smith et al. 1981, 1982), when calculated as if the satellite were a planar target at fixed gravity. Simulations by Melosh and Ryan (1997) and Benz and Asphaug (1999) indicate that catastrophic disruption is more difficult than this criterion would predict, but that a better match is found if the expected transient crater *volume* is set equal to the satellite volume. Leinhardt and Stewart (2009), in contrast, find that disruption may be easier than found by Benz and Asphaug (1999) if the target is weak. In general, we might expect somewhat different disruption thresholds depending on whether the target is solid and coherent or weak and porous, even in the gravity regime (somewhat analogous to the difference between rock/ice and sand crater scaling discussed in Section 19.5).

Equating the transient crater diameter to satellite diameter well exceeds the threshold for icy satellite *shattering*, as determined by the scaling analysis in McKinnon et al. (1991) for the mid-sized uranian satellites. We will therefore continue to use the crater-size criterion above to compute crude (but illustrative) estimates of the characteristic impact disruption times for small satellites in the Saturn system, despite some uncertainty in the literature as to how representative such a calculation is for small bodies. Table 19.2 lists disruption time scales at Saturn at current impact rates. We expect that a 400 km crater on Mimas requires a 20 km diameter impactor releasing about 10^{24} J, which exceeds the gravitational binding energy of Mimas by a factor of five. (The same energy could be dispersed by raising the temperature of a cold Mimas by a modest 50 K, which implies that disruption is not the only option[12].) *At current impact rates* Mimas experiences such events on a time scale of 50 Gyr. In any case, satellites well outside the Roche limit, such as Mimas, should be able to reassemble themselves quickly (Dobrovolskis et al. 2007). Moreover, impacts that shatter and modestly rearrange the fragments, as opposed to catastrophically dispersing more than 50% of the satellite's mass into (very) temporary saturnian orbit are equivalent from a geological perspective – the cratering record is wiped clean.

The mass of Saturn's rings is estimated to equal or exceed that of Mimas (Robbins et al. 2009), so it is interesting to ask how long a Mimas-sized satellite would last at the distance of the rings. A 20-Gyr lifetime against disruption by a $\sim$ 16-km-diameter comet seems like a reasonable requirement for an event that could not be commonplace (Lissauer et al. 1988; Dones 1993). But Table 19.2 makes it plain that the smaller number of small impactors in case A, when extrapolated to bodies tens of meters in size, leads to surprisingly long lifetimes for the very small moons such as Anthe (diameter d $\sim$ 2 km). On the other hand, Pan (d $\sim$ 28 km) and Daphnis (d $\sim$ 8 km) live within gaps in the rings, and probably would not have been able to reassemble themselves if they had been catastrophically disrupted. It is therefore comforting that their disruption timescales are not extremely short.

19.7 Observed Crater Statistics and Interpretation

The number of craters of different sizes on planetary surfaces is usually presented in the literature in two different ways (Crater Analysis Techniques Working Group 1979).

[12] It is well known that impacts partition their initial kinetic energy into both internal energy and kinetic energy of the target (Melosh 1989).

Table 19.2 Present-day catastrophic disruption time scales at Saturn

Satellite	Semi-major axis (R_s)	Diameter of catastrophic disruptor (km)	Catastrophic disruption timescales (Gyr)		
			Case A	Case B	Smith et al. (1982)
Ring parent	2.17	16	20	20	32
Pan	2.20	0.09	16	0.1	
Daphnis	2.26	0.04	3.3	1.1	
Prometheus	2.31	1.5	2.1	0.8	120
Pandora	2.35	1.2	2.8	0.9	130
Janus	2.51	4.1	4.4	3.8	200
Epimetheus	2.51	2.2	3.9	2.0	190
Mimas	3.12	20	40	40	360
Anthe	3.28	0.005	10	0.07	
Enceladus	3.94	37	180	180	360
Telesto, Calypso	4.88	0.25	16	1.8	
Helene	6.26	0.43	18	2.8	
Polydeuces	6.26	0.02	17	0.3	
Hyperion	24.6	12	230	230	2,000

The quantities given in the table include the semi-major axis of the moon in Saturn radii (R_s); the diameter of a cometary impactor, with an assumed density of 0.6 g cm^{-3}, striking the satellite at the mean impact velocity for ecliptic comets (Eq. 19.7), that would make a transient crater on a flat surface with a diameter equal to the diameter of the satellite; and the expected present-day timescales for catastrophic disruption using the Case A and Case B size distributions (Zahnle et al. 2003), and based upon rates given by Smith et al. (1982). The "ring parent" is a moon the mass of Mimas placed at the current location of Saturn's A Ring.

The first is the cumulative plot, in which the number of craters larger than diameter D per unit area, N(D), is plotted as a function of D on a log-log scale. Frequently N(D) can be approximated by a power law, $N(D) \propto D^{\gamma}$, or by a series of power laws for different size ranges. The "canonical" value of the exponent γ for primary craters is near –2 (corresponding to an index of the differential size distribution, dN/dD, of –3.) The second approach is to give a relative plot ("R-plot"), again on a log-log scale, which displays the differential size distribution of the craters. However, to enhance structure, the R-plot divides dN/dD by a power law with an index of –3. Common crater size distributions thus plot as roughly horizontal lines in R-plots. The expression plotted is $R = D_{ab}{}^3\, n/[A\,(D_b – D_a)]$, where n is the number of craters with diameters between D_b and D_a; A is the surface area of the region counted; and $D_{ab} = (D_a D_b)^{1/2}$ (see e.g., Barlow 2008). Frequently D_b is taken to be $\sqrt{2}D_a$; in that case, $R = 2^{3/4}/(\sqrt{2}-1)\,D_a{}^2\,n/A$, or $R \sim 4.06 D_a{}^2\,n/A$. In this review we will primarily use R-plots to present crater size-frequency distributions.

An R-plot giving an overview of crater statistics for saturnian satellites imaged by Cassini, the Moon, and Callisto is shown in Fig. 19.5 (Kirchoff and Schenk 2008, 2009b). The SFD curves for these heavily cratered terrains are generally *convex upwards* (except for an apparent concave upwards dip between ~75 and 250 km diameter, depending on satellite), reaching maximum values of $R \sim 0.1 – 0.3$, i.e., slightly below or above the "empirical saturation" line of Hartmann (1984). As Hartmann (1984) showed, many heavily cratered surfaces in the Solar System reach a maximum density near $R \approx 0.2$, about a factor of five below "geometric saturation" ($R = 1$) due to effects, like ejecta blanketing, that degrade and erase smaller craters well beyond crater rim crests (also see Melosh 1989, Chap. 10). Chapman and McKinnon 1986; their Fig. 19) showed, and more recently Richardson (2008) confirmed, that narrow SFDs may extend significantly above the average empirical saturation line, as is apparently true for Mimas and Dione in Fig. 19.5.

As was true for the Voyager results, Cassini images show that Rhea's SFD may depart somewhat from those of the other satellites, in being straighter with less convex curvature, more nearly characteristic of the putative Population I. In these new counts, based on far more extensive and better imagery than before, Rhea appears to have lost the transition to a somewhat steeper slope at greater than ~64-km diameter (or at least its statistical significance; Kirchoff and Schenk 2009b). Strom (1987) had taken this to be characteristic of the production population at Saturn, and Lissauer et al. (1988) argued that it indicated saturation at smaller crater sizes. A bump at ~10-km diameter, which was interpreted as the signature of population II on Rhea's high northern latitudes (see McKinnon 1990; McKinnon et al. 1991, Fig. 17), does not appear either (though we note that Rhea's north pole was not in sunlight during the Cassini prime mission). Interestingly, Iapetus' SFD bears some degree of resemblance to that of Rhea (Kirchoff and Schenk 2009b). In general, all of the observed SFDs in Fig. 19.5 may be taken to represent, at least approximately, the true production functions for cratering in the Saturn system. As demonstrated by Chapman and McKinnon (1986), even if crater populations are "saturated," they may achieve a quasi-equilibrium that expresses the production function, provided that the production function is "shallow" (relatively depleted in small craters; i.e., R is constant or increases with increasing crater diameter) and is unchanging in time.

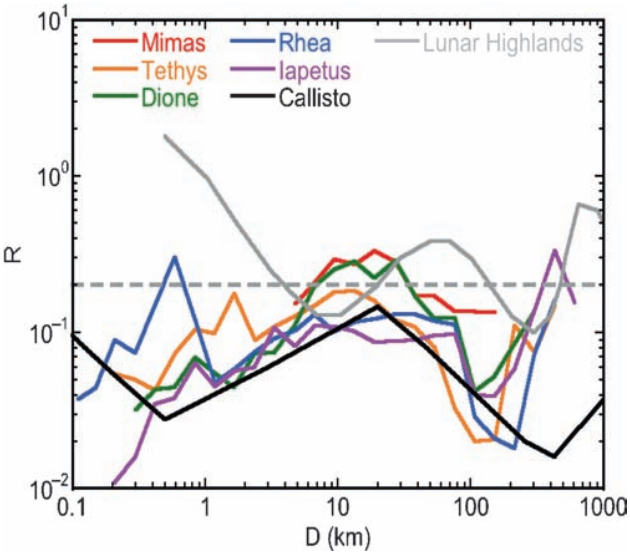

Fig. 19.5 Relative plot (R-plot) of the spatial densities of craters versus diameter for heavily cratered terrains on five satellites of Saturn (Kirchoff and Schenk 2009b), the lunar highlands (Ivanov et al. 2002), and Callisto (Schenk et al. 2004). Error bars have been omitted for clarity (see Fig. 19.6). The horizontal dashed line represents the approximate spatial density at which empirical saturation is reached according to Hartmann (1984). (Note the dip in crater densities [R values] between about 75- and 250-km diameter for these satellites and Mimas is not inconsistent, for the ≈145-km-diameter Herschel is the single crater within the "gap," and statistically speaking is consistent with a count of 1 ± 1.) The dip is remarkable because cometary impact speeds are generally much higher on the inner satellites, so there is essentially no overlap between the size of the impactors on, say, Tethys and Iapetus that would otherwise produce craters within the "dip" (see Figs. 19.3). This plot has been constructed by combining image sequences of small areas at high resolution and global mosaics at coarser resolution, the latter typically at 0.4 km pixel^{-1}. In all cases, the minimum crater size that is tabulated is about 10 pixels wide

The SFDs for the saturnian satellites appear to be broadly similar to that of Callisto, and unlike that of the Moon (although see below). Assuming a cometary chronology applies to the data shown in Fig. 19.5, Kirchoff and Schenk (2008, 2009a, b) derive *crater-retention* ages for cumulative counts of craters greater than 5- and 10-km diameter. Unless the surface is undersaturated at the diameters in question, such "ages" do not refer to the true surface age, as many more craters could have formed earlier and been destroyed. Also, these ages assume the cometary flux decreases as $1/(t - t_0)$, where $t_0 = 4.56$ Gyr (Zahnle et al. 1998), and if this is not adequate to account for the observed crater density, an age of 4.56 Gyr (the age of the Solar System) is given. For the case A cometary mass distribution described in the last section, all of the heavily cratered surfaces in Fig. 19.5 are ancient, $\approx$ 4.4–4.6 Gyr; for, case B, with more small cometary impactors, there is a range of ages, from $\approx$ 0.8 to 4.6 Gyr, with a steady increase in crater-retention age from $\approx$ 0.8 Gyr (Mimas) to 4.6 Gyr (Iapetus). In Table 19.3 we list surface ages for terrains on Mimas, Tethys, Dione, and Rhea from Kirchoff and Schenk (2008). The younger ages for the moons closer to Saturn are a consequence of the much higher predicted impact flux due to gravitational focusing of comets in the inner saturnian system. Intriguingly, the crater density on the ejecta blanket of Mimas' large central-peak "Death Star" crater Herschel is low; Kirchoff and Schenk (2009b) derive a formation age of $\approx$ 0.9 Gyr for Herschel in case A and $\approx$ 0.1 Gyr in case B. All the ages use the cometary fluxes in Zahnle et al. (2003), not the revised rates in Table 19.1; the reader can make the corresponding correction for the latter and any future revisions to the estimated cometary flux (which in any event remains highly uncertain).

Using the Neukum lunar chronology, Neukum et al. (2006) derived model ages for Iapetus from 4.2 to 4.4 Gyr; for Dione, from 3.8_2 Gyr for the "youthful" Evander basin in the southern polar region to 4.2_5 Gyr on its densely cratered plains; for Tethys, from 3.8_7 Gyr for the interior of the Odysseus basin to 4.1_2 Gyr for cratered plains east of Ithaca Chasma; and on Enceladus, from less than 4 Myr for the South Polar Terrain ("tiger stripes") to 4.1_4 Gyr for its cratered plains. Because there is no absolute calibration in the Neukum chronology, whose cratering flux is presumed to be due to captured (i.e., planetocentric) asteroids, the time scale is set by assuming that Iapetus began to retain craters at 4.4 Gyr (this, in turn, is based on theoretical models of Iapetus' internal evolution [Castillo-Rogez et al. 2007; see chapter by Matson et al.]), and no gravitational focusing is assumed. The third significant figure in the ages illustrates the formal precision of this model, but not necessarily its accuracy. In general, ages derived using the cometary chronology (Section 19.6) are younger than Neukum's (*much* younger for "case B"). However, Zahnle et al. (2003) and Kirchoff and Schenk (2008, 2009b) allow craters to be formed and retained as far back as 4.56 Gyr, compared with Neukum's upper limit of 4.4 Gyr.

Figure 19.5 shows no clear relationship between a satellite's distance from Saturn and its crater density. This may indicate that all of the heavily cratered surfaces illustrated may have reached "saturation equilibrium". In particular, at the largest sizes, the crater density is highest on Iapetus, the most distant of the regular satellites (the number of multi-hundred-km impact features is remarkable). To look into this issue in more detail, in Table 19.4 we give the number of confirmed large craters (>100-km diameter) and basins (defined as craters in excess of 300-km in diameter)[13] on the five satellites shown in Fig. 19.5 (Kirchoff and Schenk 2008,

Table 19.3 Terrain ages in Gyr

	D ≥ 5 km		D ≥ 10 km	
Satellite	A	B	A	B
Mimas	4.39	0.75	4.35	1.33
Tethys	4.56	1.66	4.44	2.10
Odysseus basin	–	–	3.76	1.06
Dione – cp	4.56	2.60	4.56	3.22
Dione – sp	4.55	1.97	4.43	1.96
Evander basin	3.62	0.60	3.61	1.00
Rhea – cp	4.56	3.05	4.56	3.67
Rhea – sp	–	–	4.48	2.47

Surface ages inferred by Kirchoff and Schenk (2008), using the chronology of Zahnle et al. (2003) for Mimas, Tethys, the Odysseus basin on Tethys, cratered plains ('cp') on Dione, smooth plains ('sp') on Dione, the Evander basin on Dione, cratered plains on Rhea, and smooth plains on Rhea.

Table 19.4 Observed and predicted numbers of large craters and basins

Satellite	Satellite diameter (km)	Number of basins with D > 300 km		Number of large craters and basins with D > 100 km
		Observed	Predicted	
Mimas	396	0	0.42	1
Tethys	1,066	2	0.69	8
Dione	1,123	2	0.45	10
Rhea	1,529	3	0.41	13
Iapetus	1,471	5	0.02	18

[13] Basins on the Moon are defined as those impact structures with two or more rings (see Schultz and Merrill 1981), such as the 320-km-diameter Schrödinger. On the midsized saturnian satellites the largest craters may or may not have rings, but in general their central floors appear more complex than a simple central peak, so we use the lunar terminology ("basins") for these magnificent structures.

2009b). We also list the number of 300-km or greater basins predicted to form in 4 Gyr at current impact rates from Zahnle et al. (2003).

If we add up the known >300-km-diameter basins on Mimas, Tethys, Dione, and Rhea, we have 7 in total, compared with 2 expected at current rates in 4 Gyr, so the results might be consistent with an early era that brought a few times more impactors in total than have fallen in the last several eons. However, Iapetus has more than 100 times the predicted number of basins in 4 Gyr at current rates. Possible explanations for the discrepancy include cratering of Iapetus by a population such as early irregular satellites that did not crater the inner moons (Nesvorný et al. 2007), or viscous relaxation on Rhea, which has a thinner lithosphere than Iapetus (Iapetus' unrelaxed shape certainly indicates a long-term, thick lithosphere; e.g., Giese et al. 2007), or simply, substantial oversaturation at these large scales on the inner satellites (or a combination of all three). Neukum et al. (2006) find a crater SFD for large craters and basins on Iapetus with a differential index of –2.2, corresponding to an impactor SFD with a power-law index of ∼–2. This impactor SFD is compatible with the known SFDs of both Kuiper Belt Objects and irregular satellites in the relevant size range of tens of km (Fuentes et al. 2009; Nicholson et al. 2008; see Fig. 19.1).

In Fig. 19.6, we show individual R-plots for Enceladus, Tethys, Dione, and Rhea from Kirchoff and Schenk (2009a, b). Enceladus shows huge variations in crater density (by a factor of at least 1000 when the South Polar Terrain [Porco et al. 2006], not shown here, is counted). Kirchoff and Schenk (2007, 2009b) note that Enceladus shows steeper dropoffs for craters with both D < 2 km and D > 6 km than do the other three satellites. This might be a signature of Population II impactors (such as are usually taken to characterize Mimas' crater population; see Fig. 19.5). Alternatively, it could be a result of endogenic modification, e.g., burial of the smallest craters by plume and E Ring material and viscous relaxation, followed by burial by plume fallout, of larger craters (Kirchoff and Schenk 2007, 2009b; Smith et al. 2007). Evidence for relaxed crater topography is provided by central peak craters that rise above the local mean elevation on Mimas, Enceladus, Tethys, and Dione, but not on Rhea and Iapetus (Schenk and Moore 2007; Dombard et al. 2007).

Tethys and Rhea are geologically inactive, at least in comparison with Enceladus and Dione. It might therefore be seen as somewhat disquieting that counts from different image sequences on Rhea in Fig. 19.6 do not always agree with each other. These discrepancies are most noticeable between the high-resolution ("hr") and global counts on Rhea. Such differences in R-values illustrate the effects of global averaging versus higher-resolution counts from very limited areas (as is the case here); the latter can be affected by unrecognized secondaries, lighting geometry, and local geological history.

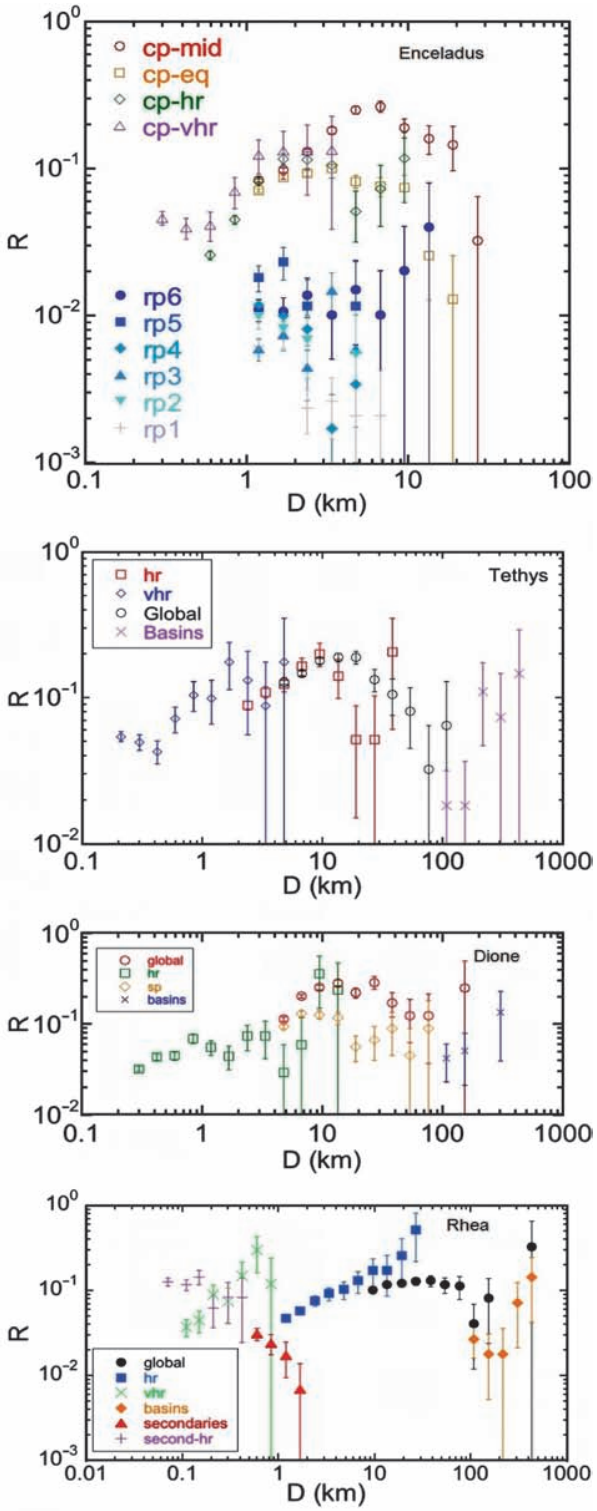

Fig. 19.6 Relative plots for terrains on Enceladus, Tethys, Dione, and Rhea (from Kirchoff and Schenk 2009b). The terrains include the heavily cratered plains ("cp") and lightly cratered ridged plains ("rp") on Enceladus (as defined by Kargel and Pozio 1996); and global counts on Tethys, Dione, and Rhea, supplemented with high-resolution ("hr") or very high-resolution ("vhr") coverage of limited areas

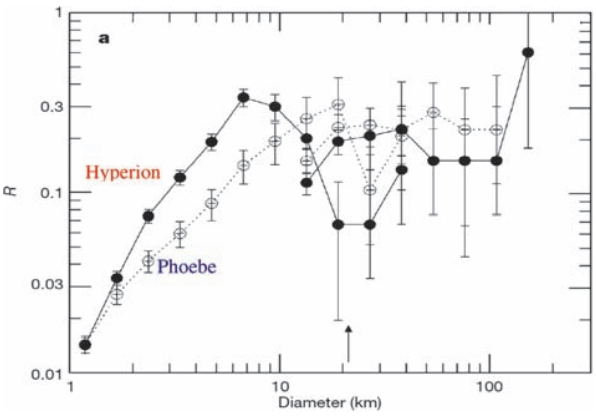

Fig. 19.7 Relative plots for Hyperion and Phoebe, from Thomas et al. (2007a). The rapid increase of R with increasing crater diameter is interpreted by Thomas et al. and by Richardson and Thomas (2007) as being due to the combined effects of a shallow impactor size distribution and erasure by larger craters. The red arrow near 20-km diameter represents the typical size of a crater made by a 1-km ecliptic comet on Hyperion (assuming solid-ice scaling, which is an approximation at best for this highly porous world)

For completeness we briefly discuss crater counts on the distant irregular satellite Phoebe, as well as those (such as they are) on Titan. Crater counts for Phoebe were presented by Porco (2005), and for Hyperion and Phoebe by Thomas et al. (2007a). In Fig. 19.7, we show the R-plots from Thomas et al., who find shallow size distributions (R rapidly increasing with crater diameter, D) for values of D between 1 and 10 km, and near empirical saturation ($R \sim 0.2$) for $D > 10$ km. Richardson and Thomas (2007) used a numerical stochastic cratering model to infer that Hyperion and Phoebe have been impacted by a population whose differential SFD has an index between –2.0 and –2.6. Extending the stochastic model of Chapman and McKinnon (1986) and Bottke (2006), Richardson and Thomas showed that an impactor population with a shallow size-frequency distribution produces a "quasi-equilibrium" paucity of small craters.

Craters on Titan are best seen by radar. Lorenz et al. (2007) list three confirmed craters: Menrva (~440 km diameter), Sinlap ($D = 80$ km) and Ksa (29 km). The USGS Astrogeology Gazetteer of Planetary Nomenclature (2009) adds two more: Afekan (115 km) and Selk (29 km). The lack of craters with $D < 20$ km was expected because of shielding by Titan's thick atmosphere (e.g., Lorenz 1997), but the rarity of 20-to-100-km features seems to imply erosion and/or burial of craters; simple observational incompleteness may also be involved. Menrva likely formed billions of years ago, but models suggest crater retention ages of 100 Myr to 1 Gyr for the mid-sized craters (Lorenz et al. 2007; Jaumann and Neukum 2009). Wood et al. (2008) find 70 possible degraded craters on the 22% of Titan's surface seen by radar as of early 2008.

19.8 Conclusions

We are in the early days of interpreting the cratering record of the saturnian satellites, but at least we now have the proper data in hand. In preparing this chapter, we have examined crater counts carried out independently by Neukum's group (Porco 2005, 2006; Thomas et al. 2007a) and by Kirchoff and Schenk (2009a, b), and the counts generally appear to be consistent in an overall cumulative sense. The devil is always in the details, though, and until all counts are published and available, it will not be possible to fully intercompare the structures of the various crater SFDs (i.e., their R-values). Moreover, convergence on the interpretation of the counts will probably remain elusive for some time to come.

Kirchoff and Schenk (2008, 2009a, b) consider the crater size-frequency distributions (SFDs) to fall into two groups, each different from the lunar highlands SFD, and attribute the satellite cratering to an outer Solar System heliocentric source. Rhea's and Iapetus' SFDs appear similar, but different from the others (Dione, Tethys, Enceladus' cratered terrain, and especially Mimas). The difference between Rhea and Mimas, in particular, was originally found by Voyager analyses and has been confirmed by all subsequent studies. These two different classes of crater SFD parallel the original Voyager-era definitions of populations I and II, but whether population II (now seen clearly only on satellites *interior* to Rhea's orbit) is truly planetocentric cannot be determined from its SFD alone.

Ecliptic comets from the Kuiper Belt are far more numerous than asteroids, at least at sizes greater than ~1 km, and the direct evidence that such comets may dominate the present-day impact rate is provided by (1) the collisions of Shoemaker-Levy 9's fragments with Jupiter and very close passages of several other comets by Jupiter, (2) observations of Saturn-crossing ecliptic comets and Centaurs (a total of 6 bodies as of this writing), and (3) the detection of the apex-antapex crater density asymmetry for younger (bright terrain) craters on Ganymede (Zahnle et al. 2001; Schenk et al. 2004). At Saturn, however, neither the strong apex-antapex asymmetries nor the steep increase in crater density as one approaches Saturn that are predicted for cometary impactors is observed. Both of these unmet expectations can be explained by crater saturation equilibrium, in that there are limits to how heavily cratered any surface, or hemisphere, can get. The lack of apex-antapex asymmetries could also result from satellite reorientation following large impacts (Lissauer 1985; Nimmo and Matsuyama 2007), and in the case of Enceladus, polar wander or other reorientation due to internal activity (Nimmo and Pappalardo 2006).

Neukum et al. (2006) take main-belt asteroids to be the primary impactors on the terrestrial planets and the satellites of Jupiter and Saturn, at least in early Solar System history, based upon common features in these bodies' crater SFDs.

For example, the maximum at 60-km diameter in the R-plot for the Moon is identified with maxima at about 12 km for Mimas, Dione, and Tethys (Fig. 19.5). The smaller crater sizes for the saturnian moons imply considerably smaller impact velocities, given by Horedt and Neukum (1984b) as ranging from 1.6 km s^{-1} for Iapetus to 5.9 km s^{-1} for Enceladus. These speeds are so small that they imply planetocentric impactors. However, no mechanism has been suggested for populating Saturn's vicinity with more bodies from the main asteroid belt than from the cometary reservoirs. Moreover, there is no known mechanism for capturing any such near-Saturn asteroids into the required low-eccentricity orbits around Saturn. We do believe, however, that planetocentric populations such as a large early population of irregular satellites and the debris of catastrophically disrupted satellites may have played important roles in the history of the Saturn system. Perhaps an earlier generation of satellites underwent an instability like that in the Nice model.

In the absence of independent radiometric dates, crater counts cannot support one proposed history of the Saturn system over another. However, continued work on crater counting, dynamical modeling, impact simulation, and crater modification and saturation processes will prepare us well for the day when we return the first sample from a moon of our Solar System's most iconic planet.

Acknowledgments We thank Nico Schmedemann, Amy Barr, Beau Bierhaus, Bill Bottke, Hal Levison, Alessandro Morbidelli, David Nesvorný, and David Vokrouhlický for discussions, and the editors for their patience. This research was supported by grants from the Cassini Data Analysis Program to LD, MRK, and WBM.

References

Alvarellos, J. L., Zahnle, K. J., Dobrovolskis, A. R., Hamill, P. 2005. Fates of satellite ejecta in the Saturn system. Icarus 178, 104–123.

Asphaug, E., Benz, W. 1996. Size, density, and structure of comet Shoemaker-Levy 9 inferred from the physics of tidal breakup. Icarus 121, 225–248.

Barlow, N. 2008. *Mars: An Introduction to its Interior, Surface and Atmosphere*. Cambridge Univ. Press, Cambridge, UK, 276 pp.

Barr, A. C., Canup, R. M. 2008. Constraints on gas giant satellite formation from the interior states of partially differentiated satellites. Icarus 198, 163–177.

Barucci, M. A., Boehnhardt, H., Cruikshank, D. P., Morbidelli, A., Eds. 2008. *The Solar System Beyond Neptune*. Univ. Arizona Press, Tucson, 632 pp.

Basaltic Volcanism Study Project 1981. *Basaltic Volcanism on the Terrestrial Planets.* Pergamon, New York. 1286 pp.

Benz, W., Asphaug, E. 1999. Catastrophic disruptions revisited. Icarus 142, 5–20.

Bernstein, G. M., Trilling, D. E., Allen, R. L., Brown, M. E., Holman, M., Malhotra, R. 2004. The size distribution of trans-Neptunian bodies. Astron. J. 128, 1364–1390. Erratum: Astron. J. 131, 2364.

Bézard, B., Lellouch, E., Strobel, D., Maillard, J.-P., Drossart, P. 2002. Carbon monoxide on Jupiter: Evidence for both internal and external sources. Icarus 159, 95–111.

Bierhaus, E. B., Chapman, C. R., Merline, W. J. 2005. Secondary craters on Europa and implications for cratered surfaces. Nature 437, 1125–1127.

Bierhaus, E. B., Chapman, C. R., Merline, W. J., Brooks, S. M, Asphaug E. 2001. Pwyll secondaries and other small craters on Europa. Icarus 153, 264–76.

Boehnhardt, H. 2004. Split comets. In *Comets II* (M. C. Festou, H. U. Keller, and H. A. Weaver, Eds.), pp. 301–316. Univ. Arizona Press, Tucson.

Bottke, W. F., Chapman, C. R. 2006. Determining the main belt size distribution using asteroid cratering records and crater saturation models. Lunar and Planetary Institute Science Conference Abstracts 37, #1349.

Bottke, W. F., Durda, D. D., Nesvorný, D., Jedicke, R., Morbidelli, A., Vokrouhlický, D., Levison, H. F. 2005. The fossilized size distribution of the main asteroid belt. Icarus 175, 111–140.

Bottke, W. F., Levison, H. F., Nesvorný, D., Dones, L. 2007. Can planetesimals left over from terrestrial planet formation produce the lunar Late Heavy Bombardment? Icarus 190, 203–223.

Bottke, W. F., Morbidelli, A., Jedicke, R., Petit, J.-M., Levison, H. F., Michel, P., Metcalfe, T. S. 2002. Debiased orbital and absolute magnitude distribution of the Near-Earth Objects.

Bottke, W. F., Nesvorný, D., Vokrouhlický, D., Morbidelli, A. 2009. The irregular satellites: The most collisionally evolved populations in the solar system. Astron. J., submitted.

Brown, M. E., Barkume, K. M., Ragozzine, D., Schaller, E. L. 2007. A collisional family of icy objects in the Kuiper Belt. Nature 446, 294–296.

Brunini, A. di Sisto, R. P., and Orellana, R. B. 2003. Cratering rate on the jovian system: The contribution from Hilda asteroids. Icarus 165, 371–378.

Buckingham, E. 1914. On physically similar systems; illustrations of the use of dimensional equations. Phys. Rev. 4, 345–376.

Castillo-Rogez, J. C., Matson, D. L., Sotin, C., Johnson, T. V., Lunine, J. I., Thomas, P. C. 2007. Iapetus' geophysics: Rotation rate, shape, and equatorial ridge. Icarus 190, 179–202.

Chapman, C. R. 1990. Crater saturation simulation. Bull. Amer. Astron. Soc. 22, 1057.

Chapman, C. R., Cohen, B. A., Grinspoon, D. H. 2007. What are the real constraints on the existence and magnitude of the late heavy bombardment? Icarus 189, 233–245.

Chapman, C. R., McKinnon, W. B. 1986. Cratering of planetary satellites. In *Satellites* (J. A. Burns and M. S. Matthews, Eds.), pp. 492–580. Univ. Arizona Press, Tucson.

Charnoz, S., Morbidelli, A., Dones, L., Salmon, J. 2009. Did Saturn's rings form during the Late Heavy Bombardment? Icarus 199, 413–428.

Collins, G. S., Davison, T., Elbeshausen, D., Wünnemann, K. 2009. Numerical simulations of oblique impacts: The effect of impact angle and target strength on crater shape. LPSC 40th, Abstract #1620.

Crater Analysis Techniques Working Group 1979. Standard techniques for presentation and analysis of crater size-frequency data. Icarus 37, 467–474.

Croft, S. K., Kargel, J. S., Kirk, R. L., Moore, J. M., Schenk, P. M., Strom, R. G. 1995. The geology of Triton. In *Neptune and Triton* (D. P. Cruikshank, Ed.), pp. 879–947. Univ. Arizona Press, Tucson.

Del Popolo, A., Gambera, M., and Ercan, N. 2001. Migration of giant planets in planetesimal discs. Mon. Not. R. Astron. Soc. 325, 1402–1410.

Di Sisto, R. P., Brunini, A. 2007. The origin and distribution of the Centaur population. Icarus 190, 224–235.

Dobrovolskis, A. R., Alvarellos, J. L., Lissauer, J. J. 2007. Lifetimes of small bodies in planetocentric (or heliocentric) orbits. Icarus 188, 481–505.

Dobrovolskis, A. R., Lissauer, J. J. 2004. The fate of ejecta from Hyperion. Icarus 169, 462–473.

Dombard, A. J., Bray, V. J., Collins, G. S., Schenk, P. M., Turtle, E. P. 2007. Relaxation and the formation of prominent central peaks in large craters on the icy satellites of Saturn. Bull. Amer. Astron. Soc. 38, 429.

Dombard, A.J., McKinnon, W. B. 2000. Long-term retention of impact crater topography on Ganymede. Geophys. Res. Lett. 27, 3663–3666.

Dones, L. 1991. A recent cometary origin for Saturn's rings? Icarus 92, 194–203.

Dones, L., Weissman, P. R., Levison, H. F., Duncan, M. J. 2004. Oort cloud formation and dynamics. In *Comets II* (M. C. Festou, H. U. Keller, and H. A. Weaver, Eds.), pp. 153–174. Univ. Arizona Press, Tucson.

Duncan, M. J., Levison, H. F. 1997. A scattered comet disk and the origin of Jupiter family comets. Science 276, 1670–1672.

Duncan, M., Levison, H., Dones, L. 2004. Dynamical evolution of ecliptic comets. In *Comets II* (M. C. Festou, H. U. Keller, and H. A. Weaver, Eds.), pp. 193–204. Univ. Arizona Press, Tucson.

Duncan, M., Quinn, T., Tremaine, S. 1988. The origin of short-period comets. Astrophys. J. Lett. 328, L69–L73.

Durda, D. D., Stern, S. A. 2000. Collision rates in the present-day Kuiper Belt and Centaur regions: Applications to surface activation and modification on comets, Kuiper Belt Objects, Centaurs, and Pluto-Charon. Icarus 145, 220–229.

Esposito, L. W. 1986. Structure and evolution of Saturn's rings. Icarus 67, 345–357.

Farinella, P., Paolicchi, P., Strom, R. G., Kargel, J. S., Zappalà, V. 1990. The fate of Hyperion's fragments. Icarus 83, 186–204.

Fernández, J. A., Ip, W.-H. 1984. Some dynamical aspects of the accretion of Uranus and Neptune – The exchange of orbital angular momentum with planetesimals. Icarus 58, 109–120.

Fernández, J. A., Morbidelli, A. 2006. The population of faint Jupiter family comets near the Earth. Icarus 185, 211–222.

Fernández, Y. 2009. Web page at http://www.physics.ucf.edu/~yfernandez/cometlist.html#jf. Accessed April 25, 2009.

Fernández, Y. R., Jewitt, D. C., Sheppard, S. S. 2002. Thermal properties of Centaurs Asbolus and Chiron. Astron. J. 123, 1050–1055.

Francis, P. J. 2005. The demographics of long-period comets. Astrophys. J. 635, 1348–1361.

Fuentes, C. I., George, M. R., Holman, M. J. 2009. A Subaru pencil-beam search for $m_R \sim 27$ trans-Neptunian bodies. Astrophys. J. 696, 91–95.

Giese, B., Denk, T., Neukum, G., Roatsch, T., Helfenstein, P., Thomas, P. C., Turtle, E. P., McEwen, A., Porco, C. C. 2008. The topography of Iapetus' leading side. Icarus 193, 359–371.

Giese, B., Neukum, G., Roatsch, T., Denk, T., and Porco, C. C. 2006. Topographic modeling of Phoebe using Cassini images. Planet Space Sci. 54, 1156–1166.

Giese, B., Wagner, R., Roatsch, T., Denk, T., Neukum, G. 2007. The topographies of Rhea and Iapetus in comparison. American Geophysical Union, Fall Meeting 2007, abstract #P12B-07AGU.

Gladman, B. J., Davis, D. R., Neese, C., Jedicke, R., Williams, G., Kavelaars, J. J., Petit, J.-M., Scholl, H., Holman, M., Warrington, B., Esquerdo, G., Tricarico, P. 2009. On the asteroid belt's orbital and size distribution. Icarus 202, 104–118.

Gladman, B., Kavelaars, J. J., Petit, J.-M., Morbidelli, A., Holman, M. J., Loredo, T. 2001. The structure of the Kuiper Belt: Size distribution and radial extent. Astron. J. 122, 1051–1066.

Gladman, B., Marsden, B. G., VanLaerhoven, C. 2008. Nomenclature in the outer Solar System. In *The Solar System Beyond Neptune* (M. A. Barucci, H. Boehnhardt, D. P. Cruikshank, and A. Morbidelli, Eds.), pp. 43–57. Univ. Arizona Press, Tucson.

Gomes, R., Levison, H. F., Tsiganis, K., Morbidelli, A. 2005. Origin of the cataclysmic Late Heavy Bombardment period of the terrestrial planets. Nature 435, 466–469.

Gomes, R. S., Morbidelli, A., Levison, H. F. 2004. Planetary migration in a planetesimal disk: Why did Neptune stop at 30 AU? Icarus 170, 492–507.

Groussin, O., Lamy, P., Jorda, L. 2004. Properties of the nuclei of Centaurs Chiron and Chariklo. Astron. Astrophys. 413, 1163–1175.

Hahn, G., Lagerkvist, C.-I., Karlsson, O., Oja, T., Stoss, R. M. 2006. P/2004 A1 (Loneos) – A comet under transition from Saturn to Jupiter. Astronomische Nachrichten 327, 17–20.

Hahn, J.M., Malhotra, R. 1999. Orbital evolution of planets embedded in a planetesimal disk. Astron. J. 117, 3041–3053.

Harrington, J., de Pater, I., Brecht, S. H., Deming, D., Meadows, V., Zahnle, K., Nicholson, P. D. 2004. Lessons from Shoemaker-Levy 9 about Jupiter and planetary impacts. In *Jupiter – The Planet, Satellites and Magnetosphere* (Fran Bagenal, Timothy E. Dowling, William B. McKinnon, Eds.), pp. 159–184. Cambridge Univ. Press, Cambridge, UK.

Hartmann, W. K. 1965. Terrestrial and lunar flux of large meteorites in the last two billion years. Icarus 4, 157–165.

Hartmann, W. K. 1966. Early lunar cratering. Icarus 5, 406–418.

Hartmann, W. K. 1984. Does crater "saturation equilibrium" occur in the Solar System? Icarus 60, 56–74.

Hartmann, W. K., Neukum, G. 2001. Cratering chronology and the evolution of Mars. Space Sci. Rev. 96, 165–194.

Hartmann, W. K., Ryder, G., Dones, L., Grinspoon, D. 2000. The time-dependent intense bombardment of the primordial Earth/Moon system. In *Origin of the Earth and Moon* (R. M. Canup and K. Righter, Eds.), pp. 493–512. Univ. Arizona Press, Tucson.

Holman, M. J., Wisdom, J. 1993. Dynamical stability in the outer Solar System and the delivery of short period comets. Astron. J. 105, 1987–1999.

Holsapple, K. A. 1993. The scaling of impact processes in planetary sciences. Ann. Rev. Earth Planet. Sci. 21, 333–373.

Holsapple, K. A. 2009. Web pages at http://keith.aa.washington.edu/craterdata/scaling/index.htm and http://keith.aa.washington.edu/craterdata/scaling/theory.pdf. Accessed April 25, 2009.

Holsapple, K. A., Schmidt, R. M. 1982. On the scaling of crater dimensions. II – Impact processes. J. Geophys. Res. 87, 1849–1870.

Horedt, G. P., Neukum, G. 1984a. Cratering rate over the surface of a synchronous satellite. Icarus 60, 710–717.

Horedt, G. P., Neukum, G. 1984b. Planenetocentric versus heliocentric impacts in the jovian and saturnian satellite system. J. Geophys. Res. 89**,** 10,405–10,410.

Horner, J., N.W. Evans, and M.E. Bailey 2004. Simulations of the population of Centaurs II: Individual objects. Mon. Not. R. Astron. Soc. 355, 321–329.

Housen, K. R., Holsapple, K. A. 2003. Impact cratering on porous asteroids. Icarus 163, 102–119.

Irwin, M., Tremaine, S., Żytkow, A. N. 1995. A search for slow-moving objects and the luminosity function of the Kuiper Belt. Astron. J. 110, 3082–3092.

Ivanov, B. A., Neukum, G., Bottke, W. F., Jr., Hartmann, W. K. 2002. The comparison of size-frequency distributions of impact craters and asteroids and the planetary cratering Rate. In *Asteroids III* (W. F. Bottke Jr., A. Cellino, P. Paolicchi, and R. P. Binzel, Eds.), pp. 89–101. Univ. Arizona Press, Tucson.

Jaumann, R., Neukum, G. 2009. The surface age of Titan. Lunar and Planetary Institute Science Conference Abstracts 40, abstract #1641.

Jewitt, D. 2008. Kuiper Belt and comets: An observational perspective. *Saas-Fee Advanced Course 35: Trans-Neptunian Objects and Comets* (K. Altwegg, W. Benz, and N. Thomas, Eds.), pp. 1–78. Springer, New York.

Jewitt, D. C., Trujillo, C. A., Luu, J. X. 2000. Population and size distribution of small jovian Trojan asteroids. Astron. J. 120, 1140–1147.

Johnson, T. V. 1978. The galilean satellites of Jupiter – Four worlds. Ann. Rev. Earth Planet. Sci. 6, 93–125.

JPL Solar System Dynamics 2009. Web page at http://ssd.jpl.nasa.gov/?satellites. Accessed April 25, 2009.

JPL Solar System Dynamics Small-Body Data Browser 2009. Web page at http://ssd.jpl.nasa.gov/sbdb.cgi. Accessed April 25, 2009.

Jutzi, M., Benz, W., Michel, P. 2008. Numerical simulations of impacts involving porous bodies. I. Implementing sub-resolution porosity in a 3D SPH hydrocode. Icarus 198, 242–255.

Jutzi, M., Michel, P., Hiraoka, K., Nakamura, A. M., Benz, W. 2009. Numerical simulations of impacts involving porous bodies: II. Comparison with laboratory experiments. Icarus 201, 802–813.

Kargel, J. S., Pozio, S. 1996. The volcanic and tectonic history of Enceladus. Icarus 119, 385–404.

Kary, D. M., Dones, L. 1996. Capture statistics of short-period comets: Implications for comet D/Shoemaker-Levy 9. Icarus 121, 207–224.

Kenyon, S. J., Bromley, B. C., O'Brien, D. P., Davis, D. R. 2008. Formation and collisional evolution of Kuiper Belt objects. In *The Solar System Beyond Neptune* (M. A. Barucci, H. Boehnhardt, D. P. Cruikshank, and A. Morbidelli, Eds.), pp. 293–313. Univ. Arizona Press, Tucson.

Kirchoff, M. R., Schenk, P. M. 2007. Impact crater distributions on the saturnian satellites from Cassini ISS imaging – Implications for geologic Histories and ages. Amer. Geophys. Union Fall Meeting Abstracts 545.

Kirchoff, M. R., Schenk, P. M. 2008. Bombardment history of the saturnian satellites. Workshop on Early Solar System Impact Bombardment, LPI Contrib. 1439, abstract #3023.

Kirchoff, M. R., Schenk, P. M. 2009a. Crater modification and geologic activity in Enceladus' heavily cratered plains: Evidence from the impact crater distribution. Icarus 202, 656–668.

Kirchoff, M. R., Schenk, P. M. 2009b. Impact cratering records of the mid-sized, icy saturnian satellites. Submitted to Icarus.

Lagerkvist, C.-I., Hahn, G., Karlsson, O., Carsenty, U. 2000. The orbital history of two periodic comets encountering Saturn. Astron. Astrophys. 362, 406–409.

Lamy, P. L., Toth, I., Fernández, Y. R., Weaver, H. A. 2004. The sizes, shapes, albedos, and colors of cometary nuclei. *Comets II* (M. C. Festou, H. U. Keller, and H. A. Weaver, Eds.), pp. 223–264. Univ. Arizona Press, Tucson.

Laskar, J. 1996. Large scale chaos and marginal stability in the Solar System. Cel. Mech. Dyn. Astron. 64, 115–162.

Leinhardt, Z. M., Richardson, D. C., Lufkin, G., Haseltine, J. 2009. Planetesimals to protoplanets II: Effect of debris on terrestrial planet formation. Mon. Not. R. Astron. Soc. 396, 718–728.

Leinhardt, Z. M., Stewart, S. T. 2009. Full numerical simulations of catastrophic small body collisions. Icarus 199, 542–559.

Lellouch, E., Bézard, B., Moreno, R., Bockelée-Morvan, D., Colum, P., Crovisier, J., Festou, M., Gautier, D., Marten, A., Paubert, G. 1997. Carbon monoxide in Jupiter after the impact of comet Shoemaker-Levy 9. Planet. Space Sci. 45, 1203–1212.

Lellouch, E., Moreno, R., Paubert, G. 2005. A dual origin for Neptune's carbon monoxide? Astron. Astrophys. 430, L37–L40.

Levison, H. F. 1996. Comet taxonomy. In *Completing the Inventory of the Solar System* (T.W. Rettig and J.M. Hahn, Eds.), pp. 173–191. Astron. Soc. Pac. Conf. Proc., vol. 107, Astronomical Society of the Pacific, San Francisco.

Levison, H. F., Dones, L., Chapman, C. R., Stern, S. A., Duncan, M. J., Zahnle, K. 2001. Could the lunar "Late Heavy Bombardment" have been triggered by the formation of Uranus and Neptune? Icarus 151, 286–306.

Levison, H. F., Duncan, M. J. 1997. From the Kuiper Belt to Jupiter-family comets: The spatial distribution of ecliptic comets. Icarus 127, 13–32.

Levison, H. F., Duncan, M. J., Zahnle, K., Holman, M., Dones, L. 2000. Note: Planetary impact rates from ecliptic comets. Icarus 143, 415–420.

Levison, H. F., Lissauer, J. J., Duncan, M. J. 1998. Modeling the diversity of outer planetary systems. Astron. J. 116, 1998–2014.

Levison, H. F., Morbidelli, A., VanLaerhoven, C., Gomes, R., Tsiganis, K. 2008. Origin of the structure of the Kuiper Belt during a dynamical instability in the orbits of Uranus and Neptune. Icarus 196, 258–273.

Levison, H. F., Thommes, E., Duncan, M. J., Dones, L. 2004. A fairy tale about the formation of Uranus and Neptune and the lunar Late Heavy Bombardment. In *Debris Disks and the Formation of Planets* (L. Caroff, L. J. Moon, D. Backman, and E. Praton, Eds.), ASP Conference Series 324, pp. 152–167. San Francisco, Astronomical Society of the Pacific.

Lissauer, J. J. 1985. Can cometary bombardment disrupt synchronous rotation of planetary satellites? J. Geophys. Res. 90, 11289–11293.

Lissauer, J. J., Squyres, S. W., Hartmann, W. K. 1988. Bombardment history of the Saturn system. J. Geophys. Res. 93, 13776–13804.

Lorenz, R.D. 1997. Impacts and cratering on Titan: A pre-Cassini view. Planet. Space Sci. 45, 1009–1019.

Lorenz, R. D., and 11 colleagues 2007. Titan's young surface: Initial impact crater survey by Cassini RADAR and model comparison. Geophys. Res. Lett. 34, L07204.

Lykawka, P. S., Horner, J. A., Jones, B. W., Mukai, T. 2009. Origin and dynamical evolution of Neptune Trojans – I: Formation and planetary migration. Submitted to Mon. Not. R. Astron. Soc.

Malhotra, R., 1993. The origin of Pluto's peculiar orbit. Nature 365, 819–821.

Marchi, S., Mottola, S., Cremonese, G., Massironi, M., Martellato, E. 2009. A new chronology for the Moon and Mercury. Astron. J. 137, 4936–4948.

Mazeeva, O. A. 2007. Long-period comet flux in the planetary region: Dynamical evolution from the Oort cloud. Solar System Research 41, 118–128.

McEwen, A. S., Bierhaus, E. B. 2006. The importance of secondary cratering to age constraints on planetary surfaces. Ann. Rev. Earth Planet. Sci. 34, 535–567.

McKinnon, W. B. 1990. Planetary evolution: The Hyperion hypothesis. Nature 346, 414–415.

McKinnon, W. B. 2007. The mechanics of complex crater and ringed basin formation: Constraints from 30 years of planetary observations. Bridging the Gap II: Effect of Target Properties on the Impact Cratering Process, LPI Contrib. 1360, abstract #8072.

McKinnon, W. B., Chapman, C. R., Housen, K. R. 1991. Cratering of the Uranian satellites. In *Uranus* (J.T. Bergstralh, E. D. Miner, and M. S. Matthews, Eds.), pp. 629–692. Univ. Arizona Press, Tucson.

McKinnon, W. B., Schenk, P. M., Stern, S. A. 2000. New constraints on the small Kuiper Belt object population from high-resolution images of Triton. *The Transneptunian Population*, IAU 24, Joint Discussion 4, Manchester, England.

Melosh, H. J. 1989. *Impact Cratering: A Geologic Process*. Oxford University Press (Oxford Monographs on Geology and Geophysics, No. 11), 1989, 253 pp.

Melosh, H. J., Beyer, R. A. 2009. Web page at http://www.lpl.arizona.edu/tekton/crater.html. Accessed April 25, 2009.

Melosh, H. J., Ryan, E. V. 1997. Asteroids: Shattered but not dispersed. Icarus 129, 562–564.

Morbidelli, A., Levison, H. F., Gomes, R. 2008. The dynamical structure of the Kuiper belt and its primordial origin. In *The Solar System Beyond Neptune* (M. A. Barucci, H. Boehnhardt, D. P. Cruikshank, and A. Morbidelli, Eds.), pp. 275–292. Univ. Arizona Press, Tucson.

Morbidelli, A., Levison, H. F., Tsiganis, K., Gomes, R. 2005. Chaotic capture of Jupiter's Trojan asteroids in the early Solar System. Nature 435, 462–465.

Morbidelli, A., Levison, H. F., Bottke, W. F., Dones, L., Nesvorný, D. 2009. Considerations on the magnitude distributions of the Kuiper Belt and of the Jupiter Trojans. Icarus 202, 310–315.

Morbidelli, A., Tsiganis, K., Crida, A., Levison, H. F., Gomes, R. 2007. Dynamics of the giant planets of the Solar System in the gaseous protoplanetary disk and their relationship to the current orbital architecture. Astron. J. 134, 1790–1798.

Murray, N., Hansen, B., Holman, M., Tremaine, S. 1998. Migrating planets. Science 279, 69–72.

Nesvorný, D., Alvarellos, J. L. A., Dones, L., Levison, H. F. 2003. Orbital and collisional evolution of the irregular satellites. Astron. J. 126, 398–429.

Nesvorný, D., Bottke, W.F., Levison, H., Dones, L., 2002. A recent asteroid breakup in the main belt. Nature 417, 720–722.

Nesvorný, D., Vokrouhlický, D., Morbidelli, A. 2007. Capture of irregular satellites during planetary encounters. Astron. J. 133, 1962–1976.

Neukum G. 1983. *Meteoritenbombardement und Datierung planetarer Oberflächen*. Habilitation Dissertation, Ludwig-Maximilians Univ. München, Germany, 186 pp.

Neukum, G., Hiller, K. 1981. Martian ages. J. Geophys. Res. 86, 3097–3121.

Neukum, G., Ivanov, B. A., Hartmann, W. K. 2001. Cratering records in the inner Solar System in relation to the lunar reference system. Space Sci. Rev. 96, 55–86.

Neukum, G., Wagner, R. J., Denk, T., Porco, C. C., the Cassini ISS Team 2005. The cratering record of the saturnian satellites Phoebe, Tethys, Dione and Iapetus in comparison: First results from analysis of the Cassini ISS imaging data. Lunar and Planetary Institute Conference Abstracts 36, abstract #2034.

Neukum, G., Wagner, R., Wolf, U., Denk, T. 2006. The cratering record and cratering chronologies of the Saturnian satellites and the origin of impactors: results from Cassini ISS data. Euro. Planet. Sci. Conf., 610.

Neukum, G., Wagner, R., Wolf, U., Ivanov, B. A., Head, J. W. III, Pappalardo, R. T., Klemaszewski, J. E., Greeley, R., Belton, M. J. S., Galileo SSI Team 1998. Cratering chronology in the jovian system and derivation of absolute ages. Lunar and Planetary Institute Conference Abstracts 29, abstract #1742.

Neukum, G., Wagner, R., Wolf, U., the Galileo SSI Team 1999. Cratering record of Europa and implications for time-scale and crustal development. Lunar and Planetary Institute Conference Abstracts 30, abstract #1992.

Nicholson, P. D., Ćuk, M., Sheppard, S. S., Nesvorný, D., Johnson, T. V. 2008. Irregular satellites of the giant planets. In *The Solar System Beyond Neptune* (M. A. Barucci, H. Boehnhardt, D. P. Cruikshank, and A. Morbidelli, Eds.), pp. 411–424. Univ. Arizona Press, Tucson.

Nimmo, F., Matsuyama, I. 2007. Reorientation of icy satellites by impact basins. Geophysical Research Letters 34, L19203.

Nimmo, F., Pappalardo, R.T., 2006. Diapir-induced reorientation of Saturn's moon Enceladus. Nature 441, 614–616.

O'Brien, D. P., Morbidelli, A., Levison, H. F. 2006. Terrestrial planet formation with strong dynamical friction. Icarus 184, 39–58.

Ostro, S. J., Pettengill, G. H. 1978. Icy craters on the Galilean satellites. Icarus 34, 268–279.

Parker, A., Ivezić, Ž., Jurić, M., Lupton, R., Sekora, M. D., Kowalski, A. 2008. The size distributions of asteroid families in the SDSS Moving Object Catalog 4. Icarus 198, 138–155.

Petit, J-M., Kavelaars, J. J., Gladman, B., Loredo, T. 2008. Structure and evolution of Kuiper Belt Objects and dwarf planets. In *The Solar System Beyond Neptune* (M.A. Barucci, H. Boehnhardt, D. Cruikshank, and A. Morbidelli, Eds.), pp. 71–87. Univ. Arizona Press, Tucson.

Plescia, J. B., Boyce, J. M. 1985. Impact cratering history of the Saturnian satellites. J. Geophys. Res. 90, 2029–2037.

Porco, C. C., and 34 colleagues 2005. Cassini Imaging Science: Initial results on Phoebe and Iapetus. Science 307, 1237–1242.

Porco, C. C., and 24 colleagues 2006. Cassini observes the active South Pole of Enceladus. Science 311, 1393–1401.

Ragozzine, D., Brown, M. E. 2007. Candidate members and age estimate of the family of Kuiper Belt object 2003 EL61. Astron. J. 134, 2160–2167.

Richardson, J. E. 2008. Interpreting cratered terrains: A new model investigation of crater saturation conditions. AAS/Division for Planetary Sciences Meeting Abstracts 40, #09.05.

Richardson, J. E., Thomas, P. C. 2007. Modeling the cratering records of Hyperion and Phoebe: Indications of a shallow-sloped impactor population. Bull. Amer. Astron. Soc. 38, 430.

Robbins, S.J., Stewart, G.R., Lewis, M.C., Colwell, J.E., Sremčević, M. 2009. Estimating the masses of Saturn's A and B Rings from high-optical depth N-Body simulations and stellar occultations. Icarus, in press.

Roig, F., Ribeiro, A. O., Gil-Hutton, R. 2008. Taxonomy of asteroid families among the Jupiter Trojans: Comparison between spectroscopic data and the Sloan Digital Sky Survey colors. Astron. Astrophys. 483, 911–931.

Schenk, P. M., 1989. Crater formation and modification on the icy satellites of Uranus and Saturn: Depth/diameter and central peak occurrence. J. Geophys. Res. 94, 3813–3832.

Schenk, P. M., Chapman, C. R., Zahnle, K., Moore, J. M. 2004. Ages and interiors: The cratering record of the Galilean satellites. In *Jupiter. The Planet, Satellites and Magnetosphere* (Fran Bagenal, Timothy E. Dowling, William B. McKinnon, Eds.), pp. 427–456. Cambridge Univ. Press, Cambridge, UK.

Schenk, P. M., McKinnon, W. B. 2008. A gallery of multiring basins on Europa, Ganymede, and Callisto. *Large Meteorite Impacts and Planetary Evolution IV*, LPI Contrib. 1423, abstract #3107.

Schenk, P. M., Moore, J. M. 2007. Impact crater topography and morphology on saturnian mid-sized satellites. Lunar and Planetary Institute Conference Abstracts 38, abstract #2305.

Schenk, P. M., Sobieszczyk, S. 1999. Cratering asymmetries on Ganymede and Triton: From the sublime to the ridiculous. Bull. Amer. Astron. Soc. 31, 1182.

Schenk, P. M., Zahnle, K. J. 2007. On the negligible surface age of Triton. Icarus 192, 135–149.

Schmedemann, N., Neukum, G., Denk, T., Wagner, R. 2009. Impact crater size-frequency distribution (SFD) on Saturnian satellites and comparison with other Solar-System bodies. Lunar and Planetary Institute Science Conference Abstracts 40, abstract #1941.

Schmedemann, N., Neukum, G., Denk, T., Wagner, R., Hartmann, O., Michael, G. 2008. Comparison of the production size-frequency distribution (SFD) of craters on saturnian satellites with the lunar crater SFD and asteroid diameter SFD. AAS/Division for Planetary Sciences Meeting Abstracts 40, abstract #61.09.

Schmidt, R.M., Housen, K.R., 1987. Some recent advances in the scaling of impact and explosive cratering. Int. J. Impact Eng. 5, 543–560.

Schultz, P.H., Merrill, R. B., Eds., 1981. *Multi-ring Basins, Proc. Lunar Planet. Sci. 12A*. Pergamon Press, New York.

Sheppard, S. S., Trujillo, C. A. 2006. A thick cloud of Neptune Trojans and their colors. Science 313, 511–514.

Shoemaker, E. M., Hackman, R. J., Eggleton, R. E. 1963. Interplanetary correlation of geologic time. Adv. Astronaut. Sci. 88, 70–89.

Shoemaker, E. M., Shoemaker, C. S., Wolfe, R. F. 1989. Trojan asteroids – Populations, dynamical structure and origin of the L4 and L5 swarms. In *Asteroids II* (R. P. Binzel, T. Gehrels, and M. S. Matthews, Eds.), pp. 487–523. Univ. Arizona Press, Tucson.

Shoemaker, E. M., Wolfe, R. F. 1981. Evolution of the saturnian satellites: The role of impact. Lunar Planet Sci. XII, A1–A3. LPI Contribution 428, Houston, Texas.

Shoemaker, E. M., Wolfe, R. F. 1982. Cratering time scales for the galilean satellites. In *Satellites of Jupiter* (Ed. D. Morrison, Ed.), pp. 277–339. Univ. Arizona Press, Tucson.

Smith, B. A., and 26 colleagues 1981. Encounter with Saturn – Voyager 1 imaging science results. Science 212, 163–191.

Smith, B. A., and 28 colleagues 1982. A new look at the Saturn system – The Voyager 2 images. Science 215, 504–537.
Smith, B. A., and many colleagues 1986. Voyager 2 in the Uranian system: Imaging science results. Science 233, 43–64.
Smith, B. A., and many colleagues 1989. Voyager 2 in the Neptunian system: Imaging science results. Science 246, 1422–1449.
Smith, D. E., Bray, V. J., Turtle, E. P., Melosh, H. J., Perry, J. E. 2007. Studies of viscous relaxation of craters on Enceladus. LPI Contribution 1357, 127–128.
Sosa, A., Fernández, J. A. 2009. Cometary masses derived from non-gravitational forces. Mon. Not. R. Astron. Soc. 393, 192–214.
Stern, S. A., McKinnon, W. B. 2000. Triton's surface age and impactor population revisited in light of Kuiper Belt fluxes: Evidence for small Kuiper Belt Objects and recent geological activity. Astron. J. 119, 945–952.
Strom, R. G. 1981. Crater populations on Mimas, Dione and Rhea. Lunar Planet Sci. XII, A7–A9. LPI Contribution 428, Houston, Texas.
Strom, R. G. 1987. The Solar System cratering record: Voyager 2 results at Uranus and implications for the origin of impacting objects. Icarus 70, 517–535.
Strom, R. G., Malhotra, R., Ito, T., Yoshida, F., Kring, D. A. 2005. The origin of planetary impactors in the inner Solar System. Science 309, 1847–1850.
Sussman, G. J., Wisdom, J. 1992. Chaotic evolution of the Solar System. Science 257, 56–62.
Szabó, Gy. M., Ivezić, Ž., Jurić, M., Lupton, R. 2007. The properties of Jovian Trojan asteroids listed in SDSS Moving Object Catalogue 3. Mon. Not. R. Astron. Soc. 377, 1393–1406.
Thomas, P. C., and 17 colleagues 2007a. Hyperion's sponge-like appearance. Nature 448, 50–56.
Thomas, P. C., Burns, J. A., Helfenstein, P., Squyres, S., Veverka, J., Porco, C., Turtle, E. P., McEwen, A., Denk, T., Giese, B., Roatsch, T., Johnson, T. V., Jacobson, R. A. 2007b. Shapes of the saturnian icy satellites and their significance. Icarus 190, 573–584.
Thommes, E. W., Bryden, G., Wu, Y., Rasio, F. A. 2008. From mean motion resonances to scattered planets: Producing the Solar System, eccentric exoplanets, and late heavy bombardments. Astrophys. J. 675, 1538–1548.
Thommes, E. W., Duncan, M. J., Levison, H. F. 1999. The formation of Uranus and Neptune in the Jupiter-Saturn region of the Solar System. Nature 402, 635–638.
Thommes, E. W., Duncan, M. J., Levison, H. F. 2002. The formation of Uranus and Neptune among Jupiter and Saturn. Astron. J. 123, 2862–2883.
Tiscareno, M. S., Malhotra, R. 2003. The dynamics of known Centaurs. Astron. J. 126, 3122–3131.
Tsiganis, K., Gomes, R., Morbidelli, A., Levison, H. F. 2005. Origin of the orbital architecture of the giant planets of the Solar System. Nature 435, 459–461.
Turrini, D., Marzari, F., Beust, H. 2008. A new perspective on the irregular satellites of Saturn – I. Dynamical and collisional history. Mon. Not. R. Astron. Soc. 391, 1029–1051.
Turrini, D., Marzari, F., Tosi, F. 2009. A new perspective on the irregular satellites of Saturn – II. Dynamical and physical origin. Mon. Not. R. Astron. Soc. 392, 455–474.
USGS Astrogeology Gazetteer of Planetary Nomenclature 2009. Web page at http://planetarynames.wr.usgs.gov/jsp/SystemSearch2.jsp?System=Saturn. Accessed April 25, 2009.
Vokrouhlický, D., Nesvorný, D., Levison, H. F. 2008. Irregular satellite capture by exchange reactions. Astron. J. 136, 1463–1476.
Volk, K., Malhotra, R. 2008. The Scattered Disk as the source of the Jupiter family comets. Astrophys. J. 687, 714–725.
Weissman, P. R., Levison, H. 1997. The population of the trans-Neptunian region: The Pluto-Charon environment. In *Pluto and Charon* (S. A. Stern and D. J. Tholen, Eds.), pp. 559–604. Univ. Arizona Press, Tucson.
West, R. M., Hainaut, O., Smette, A. 1991. Post-perihelion observations of P/Halley. III – an outburst at R = 14.3 AU. Astron. Astrophys. 246, L77–L80.
Wetherill, G. W. 1975. Late heavy bombardment of the moon and terrestrial planets. Lunar and Planetary Science Conference 6, 1539–1561.
Wetherill, G.W. 1981. Nature and origin of basin-forming projectiles. In *Multi-ring Basins, Proc. Lunar Planet. Sci. 12A* (P. H. Schultz and R. B. Merrill, Eds.), 1–18.
Wood, C. A., Lunine, J. I., Stofan, E. R., Lorenz, R. D., Lopes, R. M. C., Radebaugh, J., Wall, S. D., Paillou, P., Farr, T. 2008. Degraded impact craters on Titan. Lunar Planet. Sci. Conf. 39, abstract #1990.
Wünnemann K., Collins, G. S., Elbeshausen D. 2008. Limitations of point-source analogy for meteorite impact and implications to crater-scaling. Large Meteorite Impacts and Planetary Evolution IV, LPI Contrib. 1423, abstract #3076.
Wünnemann K., Collins, G. S., Melosh, H. J. 2006. A strain-based porosity model for use in hydrocode simulations of impacts and implications for transient crater growthin porous targets. Icarus 180, 514–527.
Zahnle, K. J., Alvarellos, J. L., Dobrovolskis, A. R., and Hamill, P. 2008. Secondary and sesquinary impact craters on Europa. Icarus 194, 660–674.
Zahnle, K., Dones, L., Levison, H. F. 1998. Cratering rates on the galilean satellites. Icarus 136, 202–222.
Zahnle, K., Schenk, P., Levison, H., Dones, L. 2003. Cratering rates in the outer Solar System. Icarus 163, 263–289.
Zahnle, K., Schenk, P., Sobieszczyk, S., Dones, L., Levison, H. F. 2001. Differential cratering of synchronously rotating satellites by ecliptic comets. Icarus 153, 111–129.